AD-A052 140 TECHNION RESEARCH AND DEVELOPMENT FOUNDATION LTD HAI--ETC F/G 11/1
MECHANICAL BEHAVIOR OF MULTIMATERIAL COMPOSITE SYSTEMS, INTERLA--ETC(U)
OCT 77 O ISHAI, D PERETZ, S GALI DA-ERO-76-G-062

UNCLASSIFIED NL

1 OF 1
AD
A052140

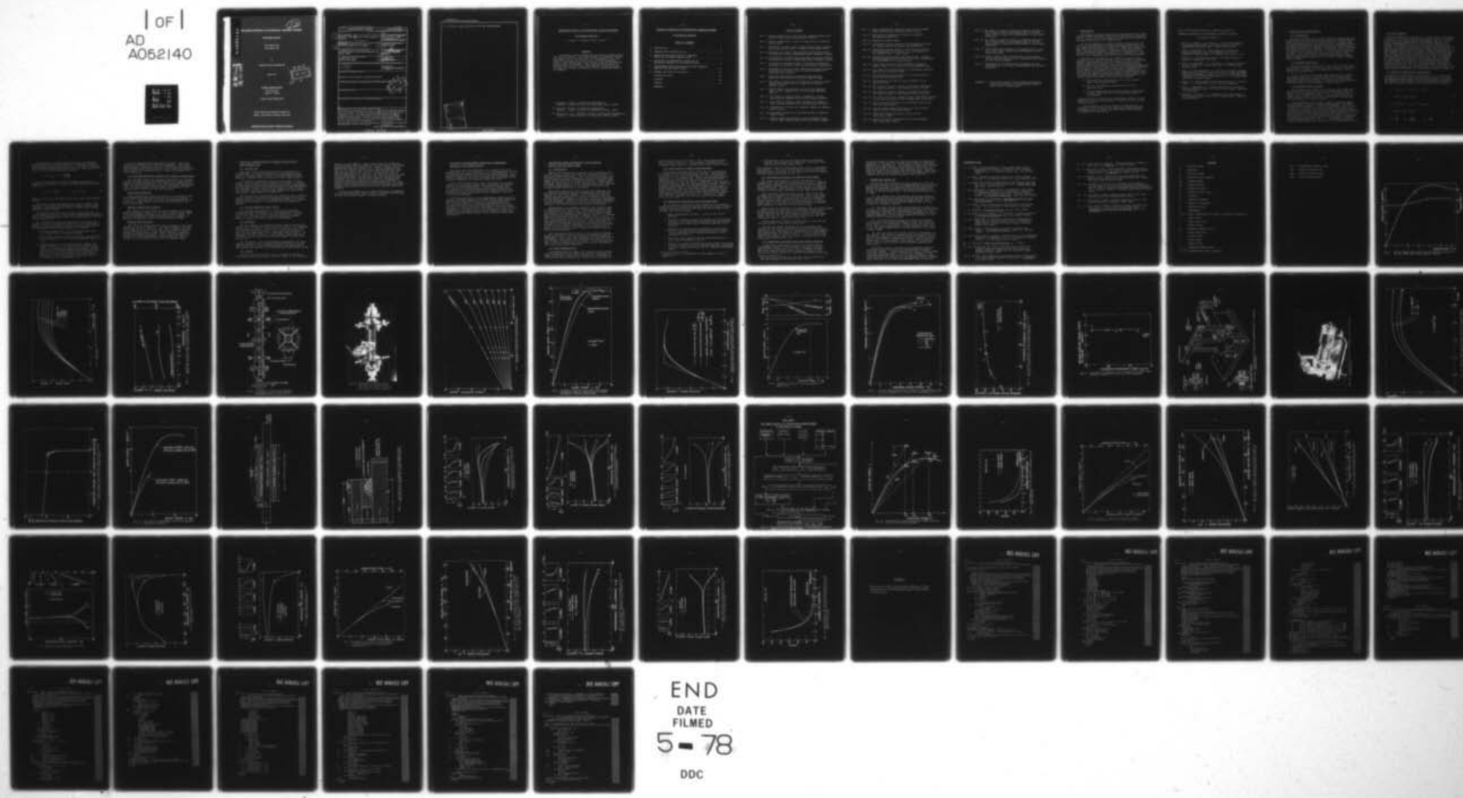

END
DATE
FILMED
5-78
DDC

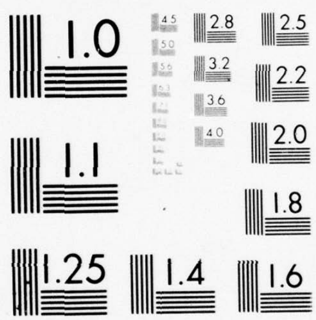
1.0
1.1
1.25
1.4
1.6
1.8
2.0
2.2
2.5
2.8
3.2
3.6
4.0
4.5
5.0

MECHANICAL BEHAVIOR OF MULTIMATERIAL COMPOSITE SYSTEMS

INTERLAMINAR BEHAVIOR

Final Technical Report

(Third Research Year)

by

Ori Ishai, Dan Peretz and Shlomit Gali

October 1977

EUROPEAN RESEARCH OFFICE
United States Army
London W. 1, England

Contract Number DAERO-76-G-062

Technion Research and Development Foundation Ltd.
Technion — Israel Institute of Technology, Haifa, Israel.

UNCLASSIFIED

SECURITY CLASSIFICATION OF THIS PAGE (When Data Entered)

RD 2355

REPORT DOCUMENTATION PAGE		READ INSTRUCTIONS BEFORE COMPLETING FORM
1. REPORT NUMBER	2. GOVT ACCESSION NO.	3. RECIPIENT'S CATALOG NUMBER
4. TITLE (and Subtitle) MECHANICAL BEHAVIOR OF MULTIMATERIAL COMPOSITE SYSTEMS, Interlaminar Behavior.		5. TYPE OF REPORT & PERIOD COVERED FINAL TECHNICAL REPORT. 1 JAN - NOV 77
		6. PERFORMING ORG. REPORT NUMBER
7. AUTHOR(s) ORI ISHAI, DAN PERETZ, SHLOMIT GALI		8. CONTRACT OR GRANT NUMBER(s) DAERO-76-G-062
9. PERFORMING ORGANIZATION NAME AND ADDRESS TECHNION RESEARCH & DEVELOPMENT FOUNDATION LTD. HAIFA, ISRAEL		10. PROGRAM ELEMENT, PROJECT, TASK AREA & WORK UNIT NUMBERS 6.11.02A-1T161102BH57-06-00-610
11. CONTROLLING OFFICE NAME AND ADDRESS US ARMY R&S GP (EUR) BOX 65, FPO NY 09510		12. REPORT DATE OCTOBER 1977
		13. NUMBER OF PAGES 71
14. MONITORING AGENCY NAME & ADDRESS (if different from Controlling Office) 74p.		15. SECURITY CLASS. (of this report) UNCLASSIFIED
		15a. DECLASSIFICATION/DOWNGRADING SCHEDULE
16. DISTRIBUTION STATEMENT (of this Report) Approved for Public Release; Distribution Unlimited		
17. DISTRIBUTION STATEMENT (of the abstract entered in Block 20, if different from Report)		
18. SUPPLEMENTARY NOTES		
19. KEY WORDS (Continue on reverse side if necessary and identify by block number)		

20. ABSTRACT (Continue on reverse side if necessary and identify by block number)

Interlaminar stress characteristics within a bonded doubler model were evaluated. The study covered the inelastic range of the adhesive up to initiation of its visco-plastic flow. The analytical solution was derived by an iterative procedure, using a linear FEM program which follows a non-linear effective stress-strain relationship. This relationship was based on uniaxial test results of the bulk adhesive, which were found to correlate with corresponding in-situ characteristics of the adhesive. (see reverse)

DD FORM 1 JAN 73 1473 EDITION OF 1 NOV 65 IS OBSOLETE

UNCLASSIFIED

SECURITY CLASSIFICATION OF THIS PAGE (When Data Entered)

388 338 4B

A final technical report dated October 1977 has been published.

MECHANICAL BEHAVIOR OF MULTIMATERIAL COMPOSITE SYSTEMS

Interlaminar Behavior

O. Ishai*, D. Peretz** and S. Gali***

ABSTRACT

Interlaminar stress characteristics within a bonded doubler model were evaluated. The study covered the inelastic range of the adhesive up to initiation of its visco-plastic flow. The analytical solution was derived by an iterative procedure, using a linear FEM program which follows a non-linear effective stress-strain relationship. This relationship was based on uniaxial test results of the bulk adhesive, which were found to correlate with the corresponding in-situ characteristics of the adhesive.

*) Professor, Faculty of Mechanical Engineering, Technion - Israel Institute of Technology, Haifa, Israel

**) Lecturer, Faculty of Mechanical Engineering, Technion - Israel Institute of Technology, Haifa, Israel

***) Instructor, D.Sc. Candidate, Faculty of Mechanical Engineering, Technion - Israel Institute of Technology, Haifa, Israel

MECHANICAL BEHAVIOR OF MULTIMATERIAL COMPOSITE SYSTEMS

Interlaminar Behavior

TABLE OF CONTENTS

LIST OF FIGURES

1. INTRODUCTION

Most modern structural adhesives are designed for high toughness and therefore exhibit highly non-linear inelastic characteristics. Hence, a non-linear program is essential for predicting structural performance of a bonded system.

Due to the complex visco-elastic-plastic nature of the IAL even at low stress levels, rigorous analytical formulation of its mechanical behavior up to failure is impossible, especially when time- and environmental factors are taken into account. Thus, comprehensive empirical information is necessary on the inelastic stress-strain relationship of the adhesive as a function of time, temperature and such factors as moisture content.

Bulk data on the adhesive may suffice so long as stress distribution and cohesive failure within the bond are concerned. However, when failure initiates or propagates close to the adhesive-adherend interfacial zone, in-situ characteristics must be taken into account and correlated with the bulk properties. Accordingly, a series of tests on the in-situ mechanical behavior of an adhesive, for different loading modes, geometries and strain rates, was conducted with a view to correlating the findings with the behavior of the bulk adhesive under uniaxial load. This goal was partly achieved and results are described in the present report which deals with three main subjects:

(a) The mechanical characteristics of the bulk epoxy used in the adhesive layer.

(b) The in-situ mechanical characteristics of the adhesive layer.

(c) The two-dimensional stress distribution (analytically solved) within the IAL at the non-linear range of the adhesive.

Preliminary tests on the in-situ hygrothermal behavior of the adhesive will be reported briefly in conjunction with a future research program.

The following is a list of reports related directly or indirectly to the output of the three-year research activity sponsored by the U.S. Army; they have either been published or submitted for publication.

List of Publications Related to Research Project on

MECHANICAL BEHAVIOR OF MULTIMATERIAL COMPOSITE SYSTEMS

Interlaminar Behavior

1. Ishai, O., Peretz, D. and Gali, S., "Direct Determination of Interlaminar Stresses in Polymeric Adhesive Layer," Experimental Mechanics, 17(7), 265-270, July 1977.

2. Ishai, O. and Gali, S., "Two-Dimensional Interlaminar Stress Distribution within the Adhesive Layer of a Symmetrical Doubler Model," J. Adhesion, 8, 301-312, 1977.

3. Peretz, D., "Interlaminar Behavior of Bonded Bimaterial Systems," Composites, July 1977.

4. Steg, I.D. and Ishai, O., "The Effect of Lateral Constraint on the Strength of a Single Lap Joint," J. Adhesion, 8, 263-273, 1977.

5. Ishai, O. and Girshengorn, T., "Strength of Bonded Aluminum-CFRP Single Lap Joint," Presented at the 9th National SAMPE Technical Conference, Atlanta, GA, Oct 4-6, 1977. Materials & Processes - In Service Performance, Vol. 9, National SAMPE Technical Conference Series.

6. Peretz, D., "Shear Stress-Strain Characteristics of Adhesive Layers," to be published in the Journal of Adhesion.

7. Gali, S. and Ishai, O., "Interlaminar Stress Distribution within an Adhesive Layer in the Non-Linear Range," submitted for publication.

8. Peretz, D. and Ishai, O., "Mechanical Characterization of Thin Adhesive Layer in-situ Under Combined Load," submitted for publication.

2. ADHESIVE BULK CHARACTERISTICS

2.1 Introduction

Bulk epoxy characteristics under different loading modes and testing conditions are currently obtained using standard experimental facilities such as the Instron tester. A ductile type of epoxy-versamid system, which was previously investigated [1-4], was selected to serve as representative for structurally tough adhesives throughout the present investigation. Most of the data is available for uniaxial tension. The purpose of the present test series was to relate this data to other loading modes such as shear. This relation will enable the prediction of the general stress-strain behavior of bulk epoxy from the elastic stage through the inelastic one up to failure, under a combined state of stress.

2.2 Specimen Fabrication

The material tested consisted of Shell epoxy epon 815 and General Mills versamid V-140 in the ratio of 70:30. The mixture was cured for 24 hours at room temperature followed by post-curing of 6 hours at 80°C.

For the tensile test, dog-bone specimens were cut from the cast plates according to ASTM D638-64T. For the shear test, thin-walled tubes were prepared and machined to have thinner thickness along the gauge length. Special metal grips were prepared and bonded to the specimens as shown in Fig. 4.

2.3 Uniaxial Tension Loading

The specimens were loaded in the Instron tester under uniaxial tension at various strain rates ranging from $15 \times 10^{-4} min^{-1}$ 38×10^{-2} at room temperature (about 22°C). A typical stress-strain curve is shown in Figure 1. The general trend for all curves shows a short linear portion beyond which a non-linear curve terminates in a stress plateau.

Other specimens were similarly loaded in uniaxial tension, and transverse strain was recorded simultaneously with longitudinal strain by means of a special extensometer. The ratio of transverse to longitudinal strains provides the Poisson ratio, ν, which is plotted as a function of uniaxial strain in Figure 1. The strain-rate effect can be evaluated from the family of stress-strain curves obtained under different strain rates (Fig. 2). The major effect is on the maximum stress plateau, S_f, which can be defined as yield stress, and shows an increase in linearity with log strain-rates [1] (Fig. 3). The effect on initial Young's modulus and proportional limit is less pronounced (Fig.3).

2.4 Shear Loading

Tubular specimens were mounted on an Instron tester and loaded in torsion. A device was designed to measure change of torsional angle, using the regular Instron extensometer (Fig. 4). The overall torsional deformation of the specimens consists of an unknown displacement at the grip region which is difficult to estimate. In order to obtain the net shear deformation along the uniform gauge length, the following procedure was carried out: Tubular specimens of different lengths, ranging from 40 to 110 mm, were loaded in torsion up to failure. Torsional displacement at each torsion moment level was plotted as a function of specimen length. These plots show a series of lines (Fig. 5) which can be extrapolated to intersect the zero length axis at different torsional displacement levels. The extrapolated shear strain at zero length, as a function of the respective shear stress (calculated from the respective torsional moment) provides the correction curve (Fig. 6). By subtraction of the correction curve from the overall shear stress-strain curve, the "true" shear stress-strain relationship can be obtained as shown in Figure 6.

2.5 Effective Stress-Strain Relationship

An effective stress-strain relationship (Fig. 7, solid curve) was derived from the uniaxial-tensile stress (Fig. 1) for the representative epoxy resin. The effective stresses and strains are related to their respective stress components by using the von Mises' deviatoric-energy yield criterion [5] as follows:

$$s = C_1[(\sigma_x-\sigma_y)^2 + (\sigma_y-\sigma_z)^2 + (\sigma_z-\sigma_x)^2$$

$$+ 6(\tau^2_{xy} + \tau^2_{yz} + \tau^2_{zx})]^{1/2} \quad (1)$$

$$e = C_2[(\varepsilon_x-\varepsilon_y)^2 + (\varepsilon_y-\varepsilon_z)^2 + (\varepsilon_z-\varepsilon_x)^2$$

$$+ 6(\varepsilon^2_{xy} + \varepsilon^2_{yz} + \varepsilon^2_{zx})]^{1/2} \quad (2)$$

$$C_1 = \frac{\sqrt{2}}{2} \qquad C_2 = \frac{\sqrt{2}}{2(1+\nu)} \qquad \varepsilon_{ij} = \frac{\gamma_{ij}}{2}$$

In the case of uniaxial tension test data, the effective stress-strain curve is identical to the respective uniaxial tensile stress-strain curve of Figure 1. In order to calculate the effective stress-strain relation from the shear tests data (Fig. 6) the following relations are used:

$$s = \sqrt{3}\,\tau_{xz} \qquad e = \frac{\sqrt{3}}{2}\,\frac{\gamma_{xz}}{1+\nu} \tag{3}$$

It has to be noted that in order to compare shear data with respective tensile data, one must use the same effective strain rate, i.e.,

$$\dot{\gamma}_{xz} = (1+\nu)\frac{2}{\sqrt{3}}\,\dot{\varepsilon}_x \qquad \dot{\gamma}_{xz} \sim \sqrt{3}\,\dot{\varepsilon}_{xy} \tag{4}$$

where $\dot{\gamma}_{xz}$ and $\dot{\varepsilon}_x$ are the shear and tensile strain rates respectively.

The plots of shear and tensile tests data in terms of the effective stress-strain relationship in Figure 7 exhibit good agreement. This supports the effective stress-strain concept used in the present study.

The analytical solution for inelastic stress distribution in the adhesive within the doubler model necessitates the derivation of the adhesive moduli as well as Poisson Ratio at the different strain levels.

The variations of effective tangent (E_t) and secant (E_s) moduli, as well as effective Poisson ratio, ν, as functions of effective strain, are shown in Figure 8. Three regions may be distinguished along the stress-strain curve, namely:

1. an almost linear region up to the proportional limit (S_ℓ) through which ν is almost constant;

2. a non-linear, probably viscoelastic range, characterized by an increase in ν, up to the "yield plateau" level (S_f);

3. a macro-plastic flow range beyond which stresses are almost constant and even tend to drop at higher strain levels. ν is almost invariant at this range. By substraction of the elastic components of axial and transverse strains, the "non-elastic Poisson ratio" may be derived. At the "yield plateau" its value tends to approach 0.5, which is the theoretical limit based on the assumption of incompressible flow.

All the characteristics described in Figures 7 and 8 are functions of loading strain rate and temperature. The present study, however, will be confined to the reference strain rate and temperature specified in Figures 1 and 7 which are considered to be typical and representative for similar "non-linear" adhesive materials.

2.6 Bulk Characteristics Compared with Adhesive In-Situ Data

In a previous report and subsequent publication [6] an investigation of shear stress-strain relationship of a similar epoxy adhesive in-situ was reported. The study was concerned with the effect of adhesive layer thickness on its mechanical characteristics. The main objective was to compare the behavior of the adhesive layer in-situ with its bulk reference.

Stress-Strain Behavior

Shear stress-strain curves for adhesives of different thickness compared with the bulk references are shown in Figures 6 and 9, The similarity of bulk to in-situ behavior is evident at the linear elastic range up to the initiation of the yield plateau level.

Adhesive Shear Elastic Modulus

The effect of in-situ adhesive layer thickness on its shear modulus is shown in Figure 10. The level of bulk modulus seems to be approximately the same as the thick adhesive layer. It may be concluded that no significant variation in modulus is apparent for adhesive layers of thicknesses above 0.3mm.

Adhesive Shear Strength

The effect of in-situ adhesive layer thickness on its shear strength is shown in Figure 11. The shear strength of the bulk epoxy seems to be on a slightly lower level compared with that of the adhesive in-situ. It may be concluded that for epoxy adhesive thickness above 0.15mm, shear strength is almost invariant with adhesive thickness. Hence, bulk shear data can be used for a first estimation of bond strength as long as failure is of the cohesive type within the adhesive layer.

3. MECHANICAL CHARACTERIZATION OF ADHESIVE LAYER IN-SITU UNDER COMBINED LOAD

3.1 Introduction

Knowledge of the mechanical properties of adhesives in a combined state of stress is essential in engineering applications of structural bonded joints in which the adhesive layer undergoes a complex state of stress even under simple loading.

Unfortunately, experimental data in this content is very scanty. Early studies of the single-lap joint model [7] tended to oversimplify the problem by assuming pure shear; subsequently, the more sophisticated closed-form solution of Goland and Reissner [8] envisaged a lateral normal stress component, the so-called "peel stress", while more recent experimental work deals mostly with cases of pure shear [6] or tension [9].

The investigation reported here was conducted using a torsion-tension apparatus to measure the mechanical properties of thin adhesive layers in-situ. Some preliminary results are presented, indicating the suitability of the method for the purpose in question.

3.2 Testing Apparatus (Figs. 12a,b)

The test specimen consists of a pair of 2025 aluminum flanged cylinders (adherends) a. The loading device consists of a torsion arm, b, operated from any conventional loading tester (e.g. Instron), and a spring operated axial loading post, c, capable of applying tension or compression.

3.3 Procedure

The test adhesive was composed of Shell epoxy resin 815 and General Mills versamid V-140 in the ratio of 70:30. The adherends were aligned on a special fixture with a controlled gap of 1mm, into which the resin was poured. The joint was cured for 24 hours at room temperature, plus 6 additional hours at 60°C. The specimens were then tested on a conventional Instron machine at different constant shear-strain rates and under different axial load levels.

For calibration, shear displacements of specimens with "zero adhesive thickness" were recorded and deducted from the overall shear displacement of the bonded specimens. The shear strains and stresses are computed from recorded moment-displacement curves.

3.4 Results

Typical shear stress-strain curves in Figure 13 indicate that normal uniaxial load has a clear-cut effect on the inelastic behavior of the adhesive. Axial tension tends to reduce the initial modulus, shear strength and ultimate strain, while axial compression tends to increase them. However, because of the lower in-situ tensile strength of the adhesive-adherend interface and its brittle mode of failure under tension load, the range of applicability is limited. Stiffness and level of yield plateau seem to be lower with the reduction in strain rate. In-situ stress-strain relationship shows fair agreement with reference bulk data. Failure under combined load may be described by means of the apparent ultimate-stress combination plotted in the shear-normal axial stress plane (Fig. 14). The failure envelope thus obtained also shows reduction of the shear strength with increasing tensile load, and increase under compression.

It may be concluded that the above methodology for adhesive in-situ characterization under combined loading can provide useful data for failure analysis of bonded systems.

4. THE EFFECT OF HYGROTHERMAL CONDITIONS ON MECHANICAL BEHAVIOR OF THE ADHESIVE LAYER.

The above topic was scheduled to be initiated only at an advanced stage of the research due to its complexity and the need for adequate experimental and analytical basic substrate. It is aimed to achieve a more realistic picture of IAL behavior under external conditions, and also to provide some information on the long-term durability of structural adhesive joints.

At the present preliminary stage, the effect of hot water immersion on the adhesive layer was investigated and compared with an oven dried counterpart. Preliminary results (Fig. 15) indicate a significant change in the shear stress-strain characteristics. The presoaked adhesive specimen showed lower stiffness, strength and ultimate strain compared to its previously dried reference.

The next step will be a more comprehensive investigation of adhesive specimens exposed to different hygrothermal conditions and tested in shear and tension in wet and dry conditions. The long range scheme is to measure hygrothermal effects on interlaminar stress and strain distributions within a doubler specimen by utilizing the method described in the Final Technical Report of the second year. The experimental results will be compared with the analytical FEM solution and will take into account the hygrothermal effects on the adhesive stress-strain relationship.

5. INTERLAMINAR STRESS DISTRIBUTION WITHIN ADHESIVE LAYER AT THE NON-LINEAR RANGE.

5.1 Introduction

Numerous publications are available on the analytical solution for stress distribution within the adhesive layer of a structural bonded joint model. Most of the earlier works [8,10-13] are based on certain assumptions such as uniform shear and normal stress distribution through the adhesive thickness which enable the derivation of a closed form solution. These simplifications, which provide only the average stress data, lead also to certain inconsistencies in the equilibrium equations and violate boundary conditions at the edges.

More recent works deal with the analytical complexity of the problem by applying numerical methods such as finite difference [14] and finite element [15-18] and provide the two-dimensional stress distribution within the adhesive layer for various bonded joint models of isotropic [15,16] and orthotropic [17,18] adherends. These solutions are in agreement with equilibrium and boundary conditions of the structural model but are limited to the elastic-linear stress-strain relationship.

Unfortunately, the polymeric adhesive layer commonly used is characterized by a non-linear stress-strain behavior, even at a relatively low stress level. This non-linearity is more pronounced at high stresses, reaching a stress plateau which may be defined as "macro-plastic" yielding (see Fig. 7). Another approach to represent this mode of behavior is by a simplified elastic-plastic model [18-20] which may provide an approximate upper bound for the real solution. Such a solution is insufficient considering the fact that under service load, the material is not allowed to approach this "yield point" and that at the critical region of the adhesive, the stress level is mainly at the non-linear range, beyond the elastic limit but below the yield plateau.

The viscoelastic-plastic nature of the polymeric adhesive, which is reflected in its sensitivity to temperature and its dependence on time [3,4], also contributes to the complexity of the problem. The present work attempts to provide the first step towards the solution of the problem. It is confined, however, to the two-dimensional case and to constant temperature and strain rate loading conditions.

5.2 Model Representation

Interlaminar adhesive layer (IAL) behavior is most conveniently represented by the symmetrical doubler model shown in Figure 16 and fully described in Reference 16. Reference 16 also provides the two-dimensional linear elastic solution for stress distribution of this model. The corresponding FEM network is shown in Figure 17. The analysis is focused on the "boundary" edge zone where stresses attain their critical value.

5.3 Plane Stress vs. Plane Strain Solutions

Plane stress and plane strain states may be considered as two bounds for the three-dimensional solution. They represent the situation close to the free edges ($y = \pm b$) and along the midsection ($y = 0$) respectively. Stress distributions based on assumptions of plane stress and plane strain for the linear range are shown in Figs. 18 and 19. Comparison of the τ_{xz} and σ_z distributions in the two cases indicated only minor variations. It may be concluded that the two-dimensional solution is not affected significantly by the unknown stresses acting along the third direction. The σ_y distribution along y derived from the plane strain solution (Fig. 20), (which may provide the upper bound for the actual three-dimensional state of stress) attains its maximum at the center line ($y = 0$). Generally it seems that the worst condition for failure would be at the corners ($y = \pm b$, $x = \pm c$).

5.4 Analytical Proceudre at the Non-linear Range

The procedure for determining the stresses at the different locations within the adhesive boundary zone under a given external uniaxial load will follow the flow chart given in Figure 21 and includes the following steps:*

1. Apply predetermined external σ_c level at the central adherend.

2. Calculate effective strains and stresses of the different elements in the FEM network using the linear FEM program and assuming the same initial effective modulus for all elements.

3. Determine the specific secant modulus at each element based on the experimental relationship given in Figures 7 and 8 according to the respective effective strain calculated in step 2.

4. Rerun the linear program with the modified modulus at each element according to step 3.

5. Compare the calculated stress S_k' at each element as derived in step 4 with the stress S_k obtained from the experimental effective stress-strain curve for the respective calculated strain.

---

* A full printout of a representative FEM program is given in Appendix 1.

6. Repeat steps 3-5 up to the stage where the difference between the calculated and "empirical" stresses is less than 2% of the final stress value.

The different steps are illustrated in Fig. 22 for a representative element k. The level of convergence was achieved by significantly fewer iterations in the case of plane strain compared with the plane stress solution (Fig. 23).

5.5 IAL Stress Distribution at the Non-linear Range

The results were focused on stress distribution at the boundary zone. The effect of axial external stress σ_C (applied to the central adherend) on the effective stress and strain at the critical point (located close to the IAL edge) is shown in Figures 24 and 25. The difference between linear and nonlinear solutions is pronounced, especially in the plane stress case.

Lower effective stress and strain were found in the case of plane strain compared with plane stress. The reverse trend was found for the shear (τ_{ZX}) and lateral normal (σ_Z) stresses as a function of axial external stress (Figure 26): namely, higher stresses in the case of non-linear solution of the plane strain state. In the case of the linear solution, no significant difference is shown for the two plane states.

Shear stress distribution at the boundary zone for σ_C=53.3 kg/mm^2 is shown in Fig.27. Here again no significant difference can be distinguished between plane stress and plane strain solutions, except at the critical location close to the lower edge corner (see Fig. 17). Similar trends were found for the two-dimentional lateral normal stress (Fig. 28).

In most cases, the effective stress tends to level off and even drop faster in the plane stress state.

The effective-stress distribution at the boundary zone (Figures 29, 30) permit evaluation of the ductile failure process of the IAL. The region of "viscoplastic flow" may comprise the elements where the effective stress or strain exceed their prespecified limit* as shown in Fig. 8. For the specific load level of the present case, this region is located close to the lower edge of the IAL (Fig. 17).

5.6 Comparison with Simplified Elasto-Plastic Solution

A simplified elasto-plastic model of the stress-strain relationship (Figure 7) has substantial advantages over the more realistic non-linear one, in that it reduces the parameters for describing the complex inelastic process to two - the initial elastic modulus E_0, and the yield-stress plateau S_f.

---

* This limit may be defined as the level where initiation of residual deformation was detected (Ref. [21]).

It may also permit inclusion of the strain-rate and temperature-dependence in the analysis, provided their effect on the above parameters is available [3]. The respective stress distributions based on this model (Figures 31-34) show that while there is no significant deviation from the exact solution at the critical location, there is some farther away from the edges. More iterations are needed for convergence of the elasto-plastic solution compared with the more exact non-linear one (Figure 35).

6. SUMMARY AND CONCLUSIONS

The present report comprises two main parts, the first of which deals with bulk and in-situ characterization of an adhesive material and provides the empirical basis for the second part, devoted to analytical solution of the stress distribution in the IAL at the non-linear range. The following conclusions may be drawn:

(a) The stress-strain relationship of the bulk adhesive under a combined state of stress may be derived from the stress-strain relationship obtained under uniaxial loading. This follows the "effective" stress-strain approach and von Mises' criteria for inelastic behavior.

(b) The shear stress-strain relationship of the adhesive in-situ, its Young's modulus and ultimate strength, may be roughly considered as invariant for thicknesses about 0.2mm; in these circumstances, bulk data provide the basic parameters for a preliminary assessment of the relevant mechanical behavior of the adhesive within a bonded structure.

(c) The finite-element method was found to be adequate for determining the stress distribution of the IAL at the non-linear range. At high external loading levels, non-linear behavior was found to predominate in narrow boundary zones close to the IAL edge, whereas most of the IAL remains at the elastic (linear) range.

(d) The non-linear FEM solution serves for assessment of IAL failure. The latter is manifested by initiation of plastic flow of the adhesive, which can be related to a specific limit point on the effective stress-strain curve. Under a given external load, a "visco-plastic" state prevails in the boundary zone of the IAL with stresses in all elements exceeding the above limit.

The present study is the first step towards more general non-linear analysis and empirical investigation of bonded structural systems. Future research will involve time-dependent non-linear stress analysis of the IAL with reference to the viscoelastic-plastic nature of the polymeric adhesive; another phase will cover the influence of environmental factors (temperature, moisture) on the above time-dependent mode of behavior.

LITERATURE CITED

1. O. Ishai, "Delayed yielding of epoxy resin under tension compression and flexure. I. Behavior under constant strain rate," J. of Applied Polymer Sci., 11, 963-981 (1967).

2. O. Ishai, "Delayed yielding of epoxy resin under constant stress," J. of Applied Polymer Sci., 11, 1863-1880 (1967).

3. O. Ishai, "The effect of temperature on the delayed yield and failure of 'plasticized' epoxy resin," Polymer Eng. and Sci., 9(2), 131-140 (1969).

4. A.E. Moehlenpah, O. Ishai and A.T. DiBenedetto, "The effect of time and temperature on the mechanical behavior of a 'plasticized' epoxy resin under different loading modes," J. of Applied Polymer Sci., 13, 1231-1245 (1969).

5. J.O. Smith and O.M. Sidebottom, Inelastic behavior of load carrying members, Wiley, p.86 (1965).

6. D. Peretz, "Shear stress-strain characteristics of adhesive layer," to be published in the Journal of Adhesion.

7. O. Volkersen, Luftfahrtforschung, 15, pp. 41-47 (1938).

8. M. Goland and E. Reissner, "The stresses in cemented joints," J. of Applied Mechanics, 11(1), pp. A17-A27 (1944).

9. E.J. Hughes and J.L Rutherford, "Study of micromechanical properties of adhesive bonded joints," Aerospace Research Center, General Precision Systems, Technical Report 3744 (1968).

10. R.W. Cornell, "Determination of stress in cemented lap joints," J. of Applied Mechanics, 20(3), pp. 355-364 (1953).

11. E.W. Kuenzi and G.H. Stevens, "Determination of the mechanical properties of adhesive for use in the design of bonded joints," U.S.-FPL Report FRL-011 (1963).

12. O. Volkersen, Construction Metalliane, 4, 3 (1965).

13. W.J. Renton and J.R. Vinson, "The analysis and design of composite material bonded joints under static and fatigue loadings," AFOSR-1760-72, Scientific Report AFOSR-TR-73-1627 (1973).

14. J. Pirvics, "Two dimensional displacement-stress distributions in adhesive bonded composite structures," J. Adhesion, 6, p. 207 (1974)

15. R.S. Alwar and Y.R. Nagaraja, "Elastic analysis of adhesive butt joint," J. Adhesion, 7, 279-287 (1976).

16. O. Ishai and S. Gali., "Two-dimensional interlaminar stress distribution within the adhesive layer of a symmetrical doubler model," J. Adhesion, 8, 801-312 (1977).

17. D. Kutscha, et al., "Feasibility of joining advanced composite flight vehicle structures," ITT Res. Int. Technical Report AFML-TR-68-391 (1969).

18. J.N. Dickson, T.M. Hsu and M.J. McKinney, "Development of an understanding of the fatigue phenomena of bonded and bolted joints in advanced filamentary composite materials," Vol. 1, Analysis Methods," Technical Report AFFDL-TR-72-64 (1972).

19. L.J. Hart-Smith, "Adhesive-bonded double-lap joints," NASA Contract Report No. NASA-CR-112235 (1973).

20. L.J. Hart-Smith, "Adhesive-bonded single-lap joints," NASA Contract Report No. NASA-CR-112236 (1973).

21. O. Ishai and S.R. Bodner, "Limits of linear viscoelasticity and yield of a filled and unfilled epoxy resin," Transactions of the Society of Rheology, 14(2), 253-273 (1970).

GLOSSARY

b - half IAL width

C - constant

c - half IAL length

E_0 - initial Young's modulus

E_s - secant modulus

E_t - tangent modulus

e - effective strain

$\dot{e}$ - effective strain rate

h - thickness

h_0 - adhesive thickness

n - number of iterations

s - effective stress

T - temperature

x, y, z - axial, transverse and lateral coordinates respectively

γ - shear strain

$\dot{\gamma}$ - shear strain rate

ε - normal strain

ε_c - uniaxial external strain

$\dot{\varepsilon}$ - axial strain rate

ν - Poisson ratio

τ - shear stress

σ - normal stress

σ_c - uniaxial external stress

$\chi = \frac{x}{c}$ - nondimensional axial coordinate

IAL	-	interlaminar adhesive layer
CAL	-	central adherend layer
EAL	-	external adherend layer
FEM	-	finite element method

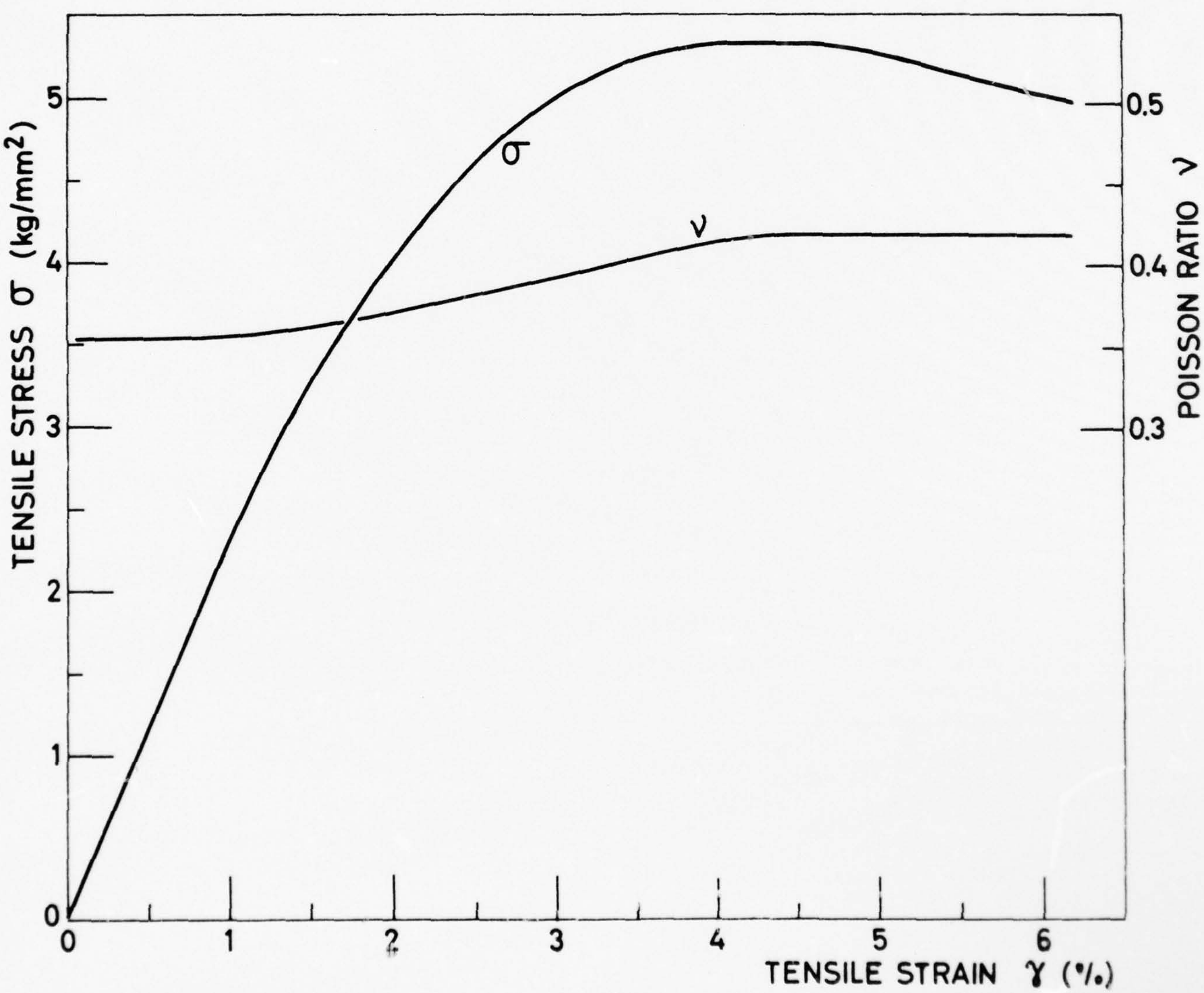

FIG. 1 TYPICAL STRESS-STRAIN CURVE AND THE RELATED POISSON RATIO FOR BULK EPOXY RESIN UNDER UNIAXIAL TENSION.

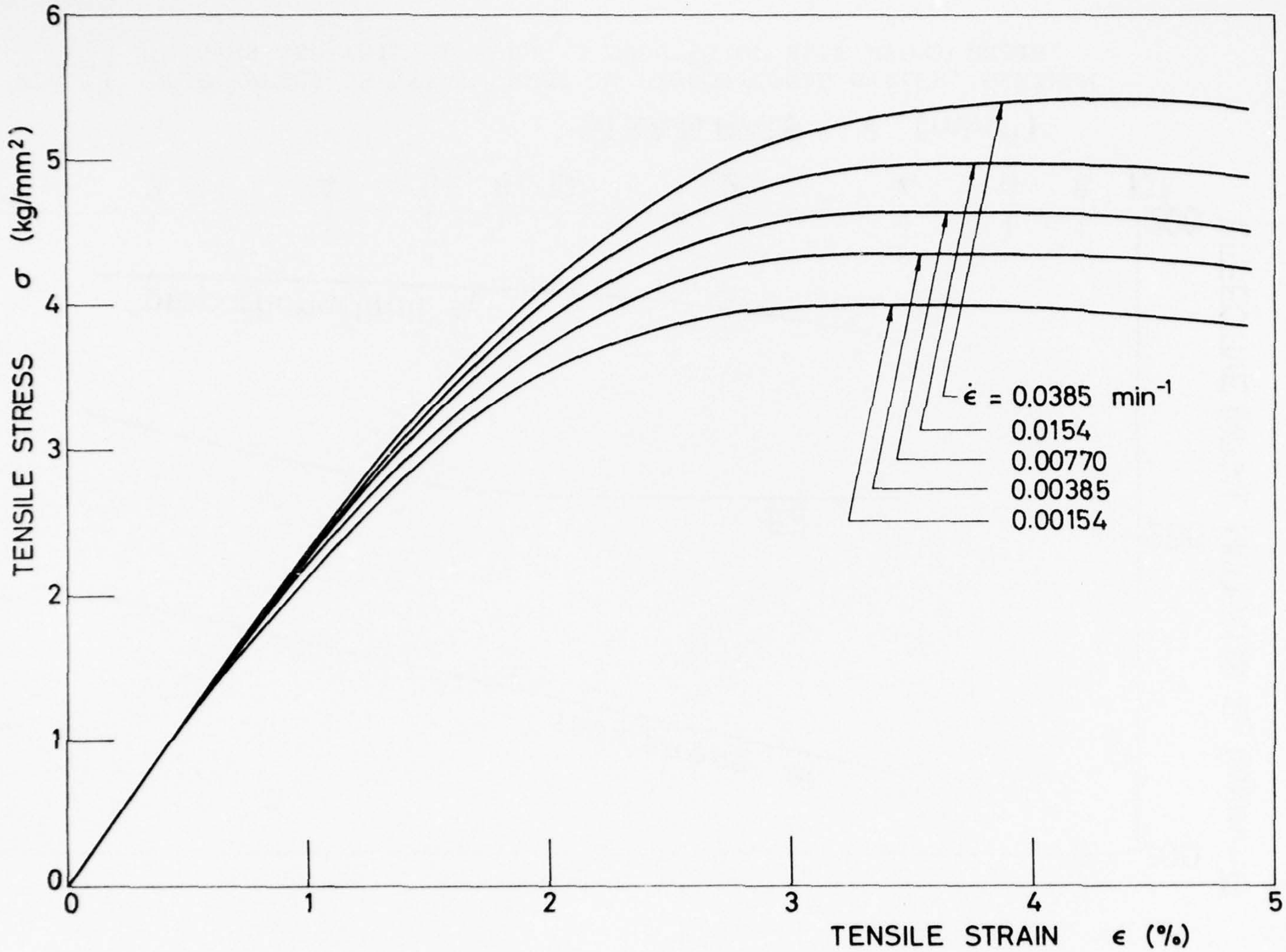

FIG. 2 TENSILE STRESS-STRAIN CURVES OF EPOXY RESIN AT DIFFERENT STRAIN RATES.

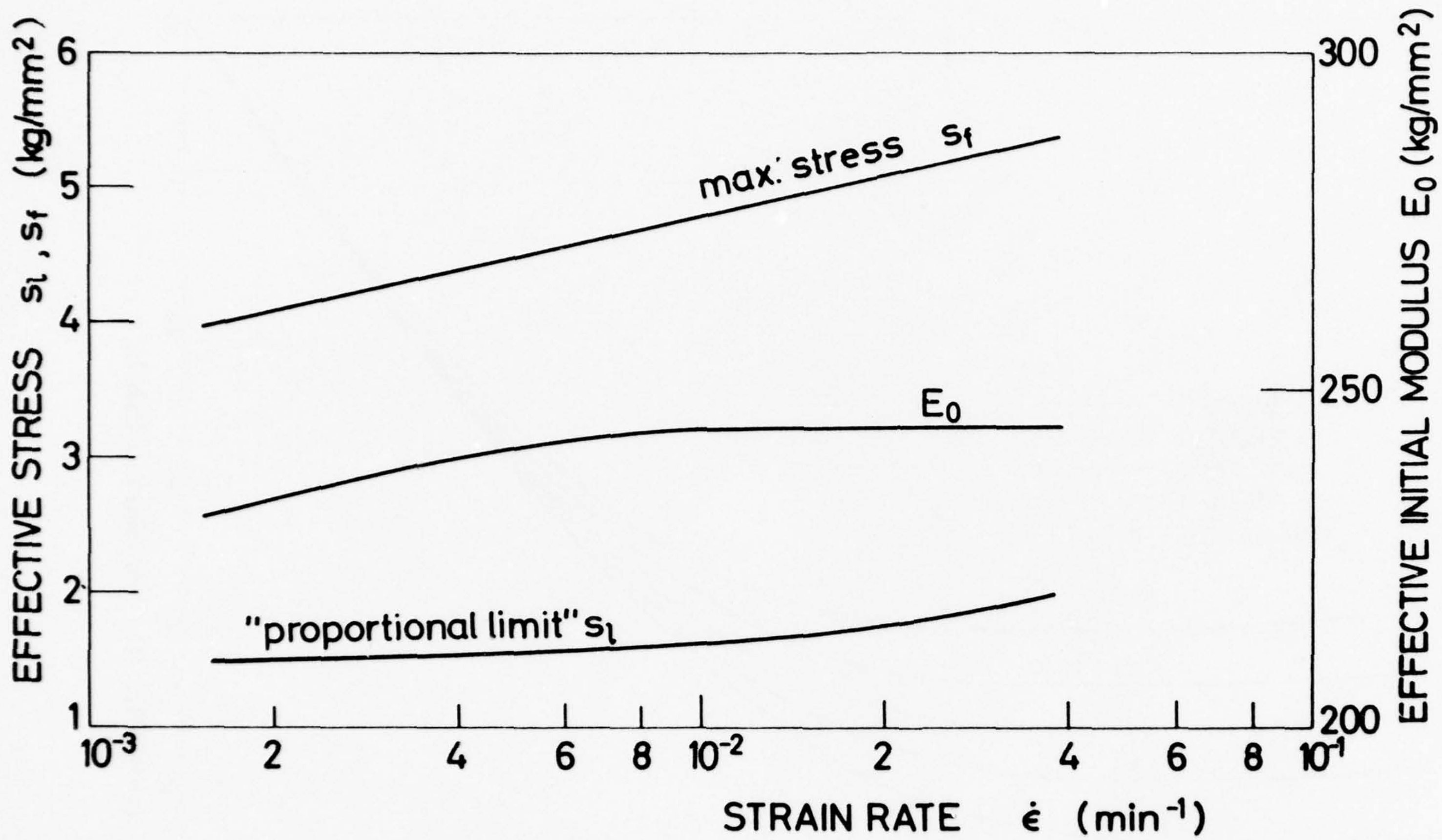

FIG. 3 THE EFFECT OF STRAIN RATE ON PROPORTIONAL STRESS, MAXIMUM STRESS AND INITIAL YOUNG'S MODULUS OF BULK EPOXY RESIN.

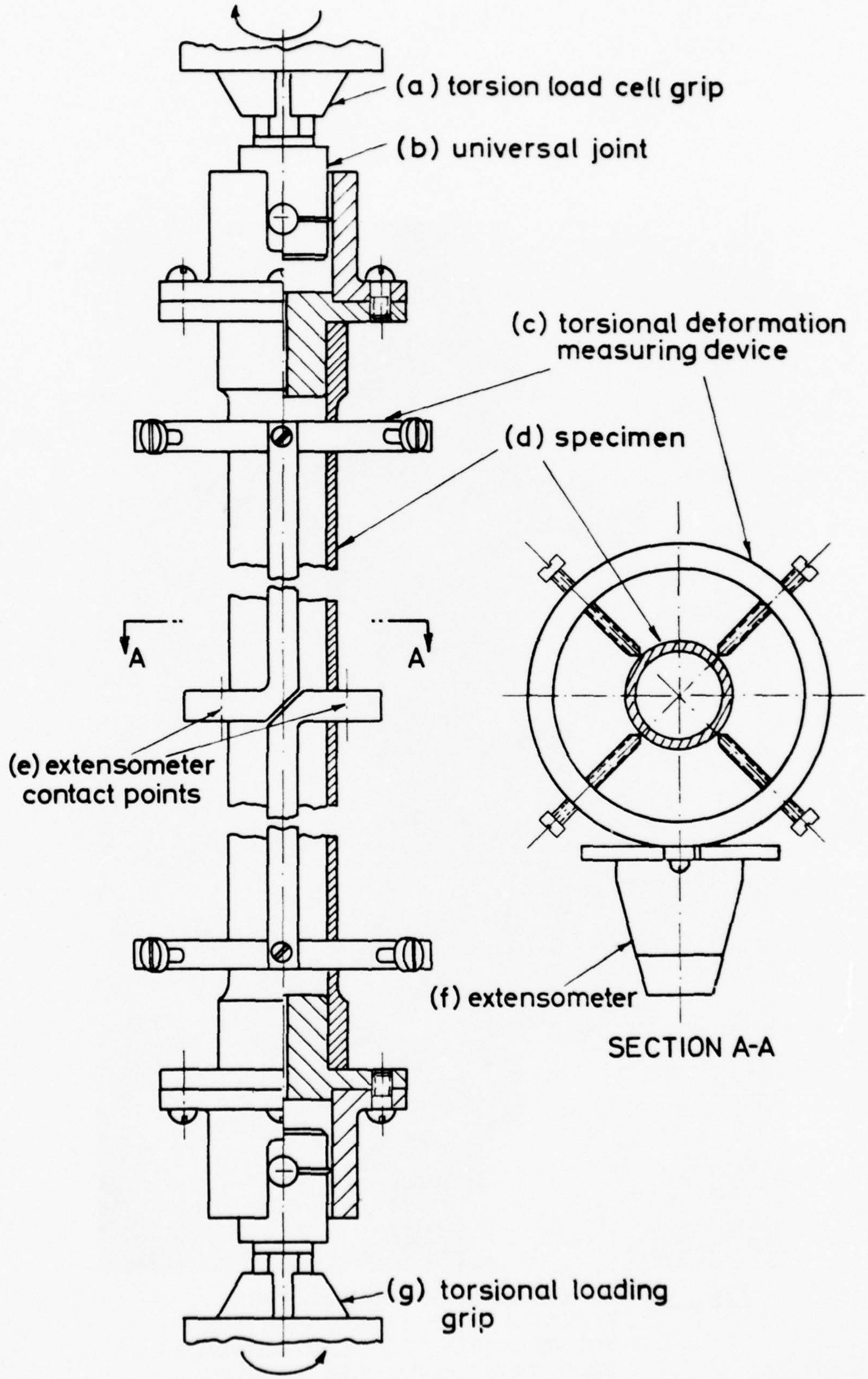

FIG. 4a ILLUSTRATION OF TUBULAR EPOXY SPECIMEN WITH SPECIAL DEVICE FOR MEASURING ANGULAR DISPLACEMENT UNDER TORSIONAL LOADING

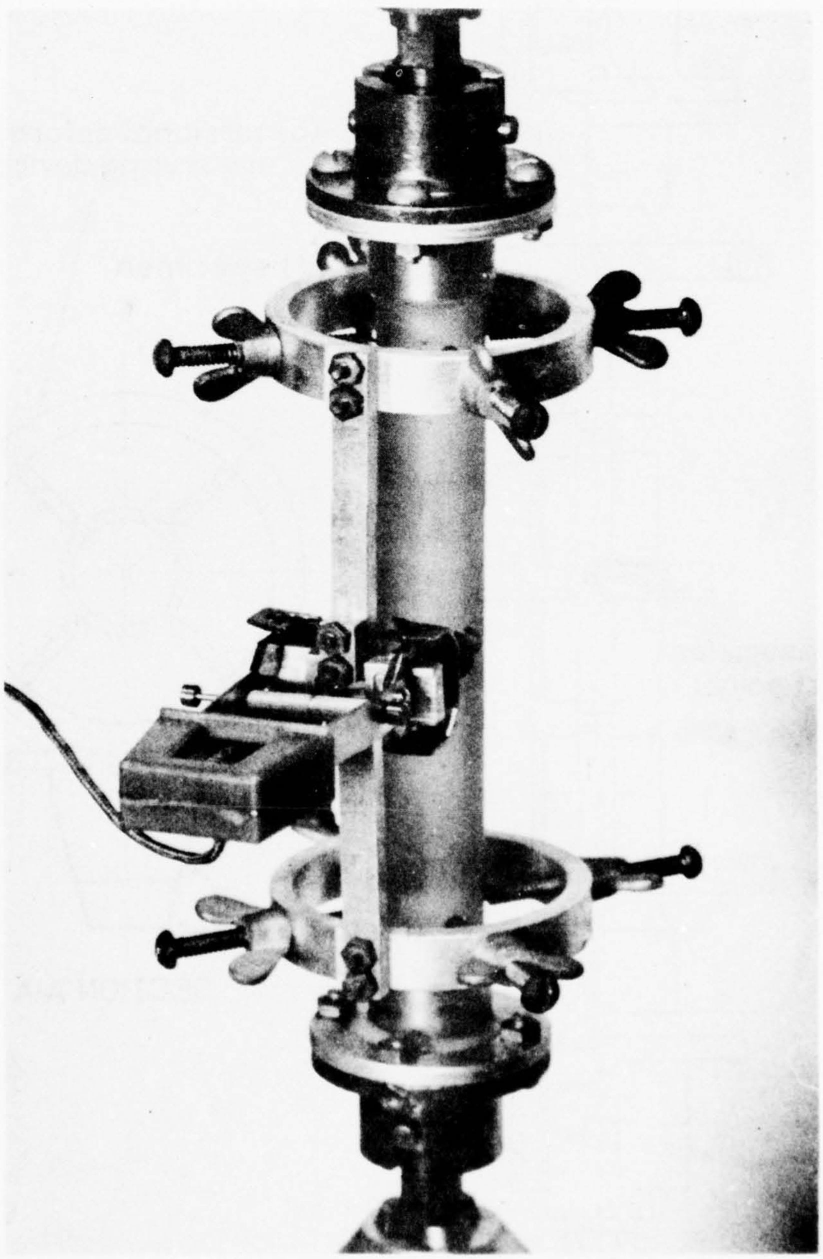

FIG. 4b PHOTOGRAPH OF TUBULAR EPOXY SPECIMEN WITH SPECIAL DEVICE FOR MEASURING ANGULAR DISPLACEMENT UNDER TORSIONAL LOADING.

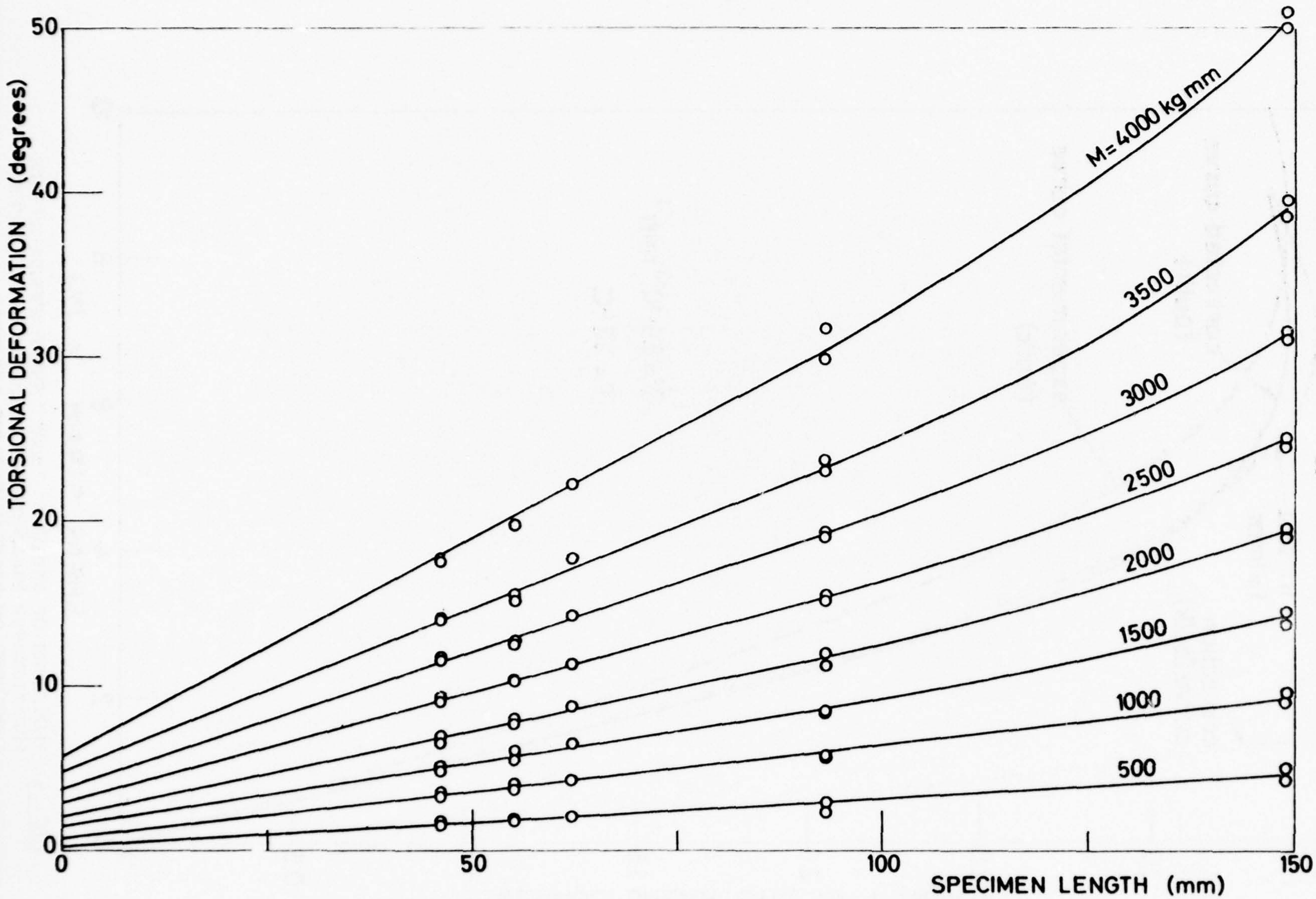

FIG. 5 THE EFFECT OF SPECIMEN LENGTH ON TORSIONAL DEFORMATION - PROCEDURE FOR CORRECTING SHEAR STRESS-STRAIN RELATIONSHIP.

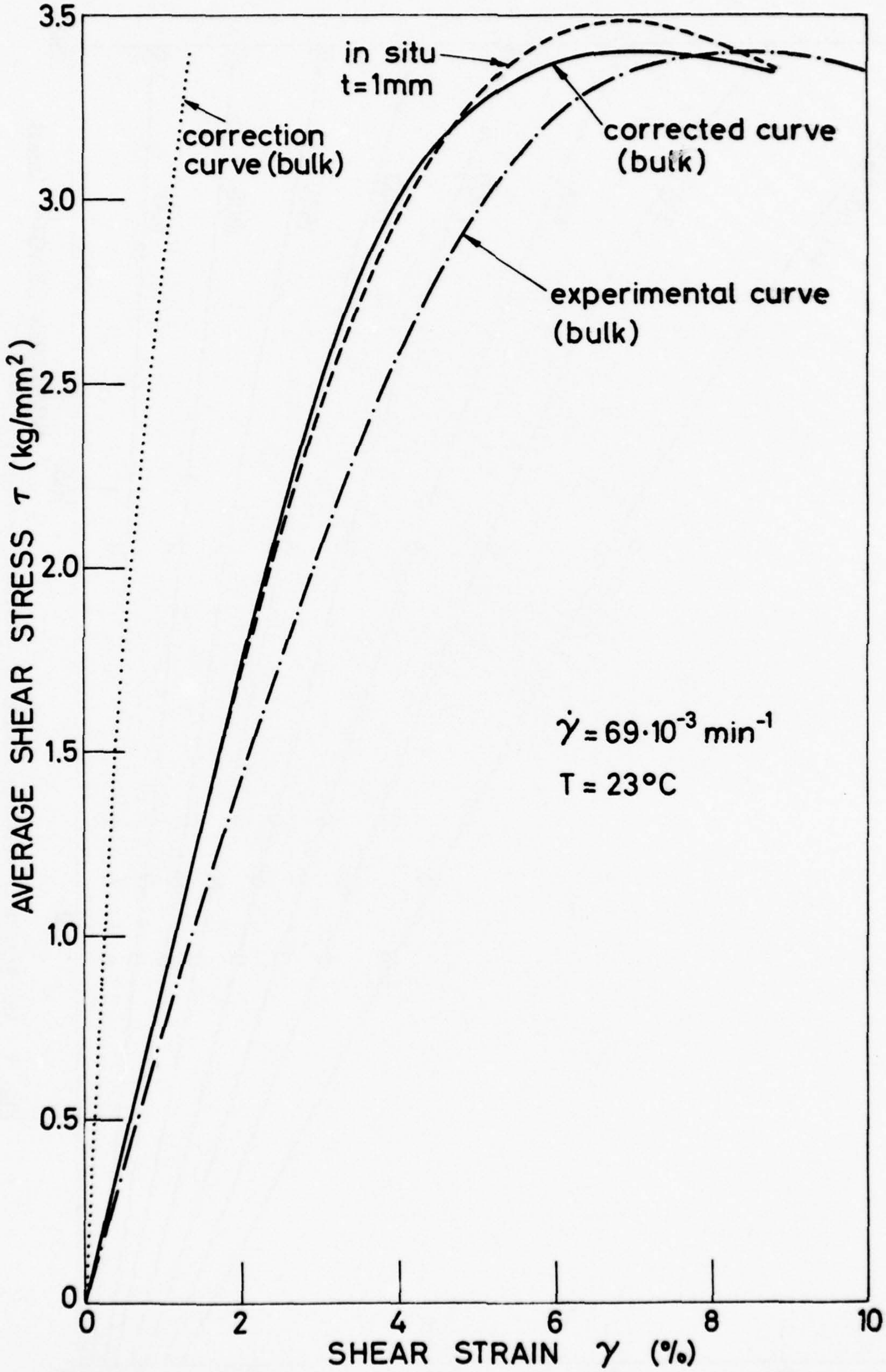

FIG. 6 PROCEDURE OF DERIVING "TRUE" SHEAR STRESS-STRAIN RELATIONSHIP BASED ON TORSIONAL TEST OF TUBULAR SPECIMENS OF DIFFERENT GAUGE LENGTHS.

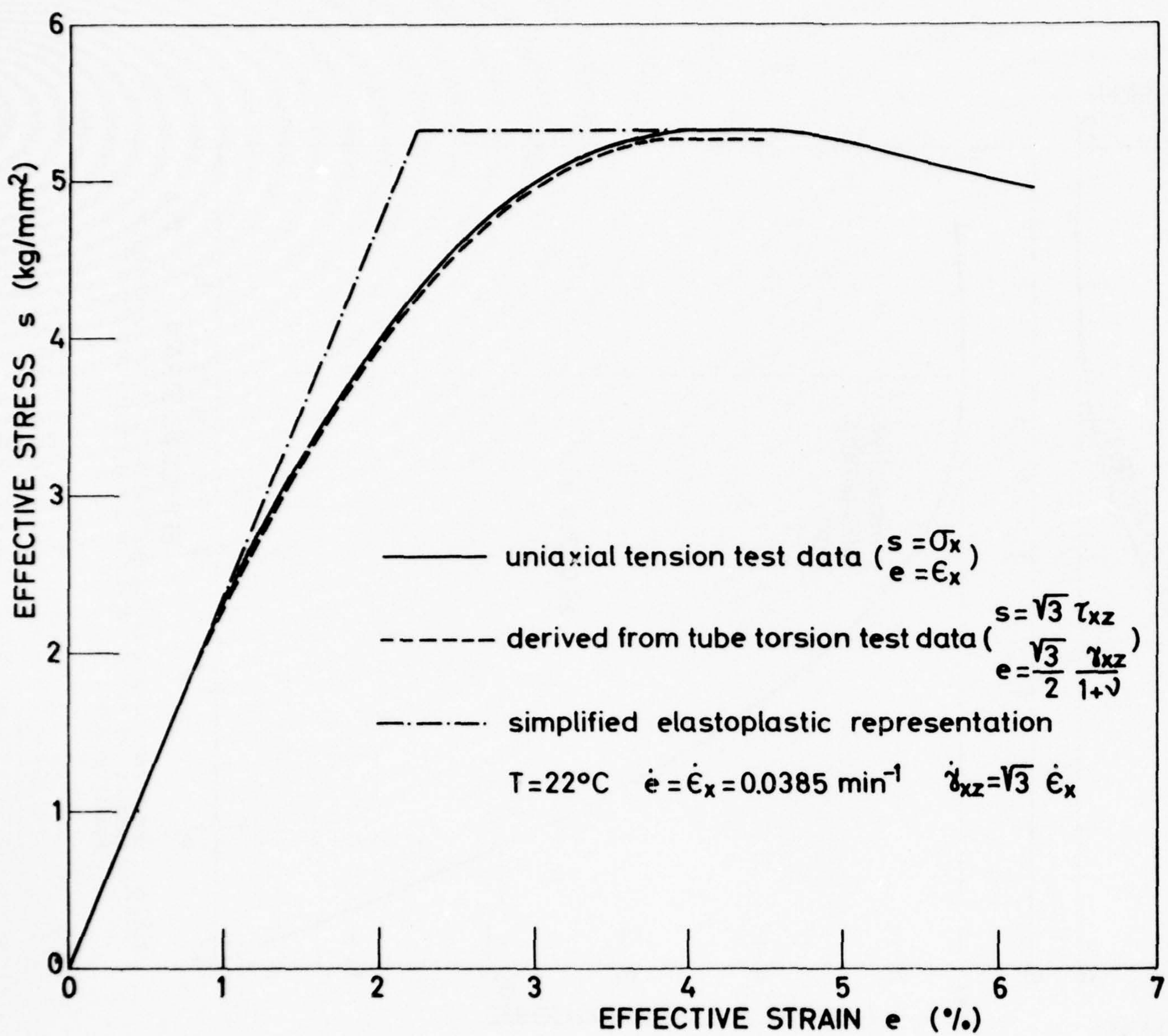

FIG. 7 EFFECTIVE STRESS-STRAIN RELATIONSHIP AND RELATED PROPERTIES FOR EPOXY RESIN USED AS ADHESIVE LAYER.

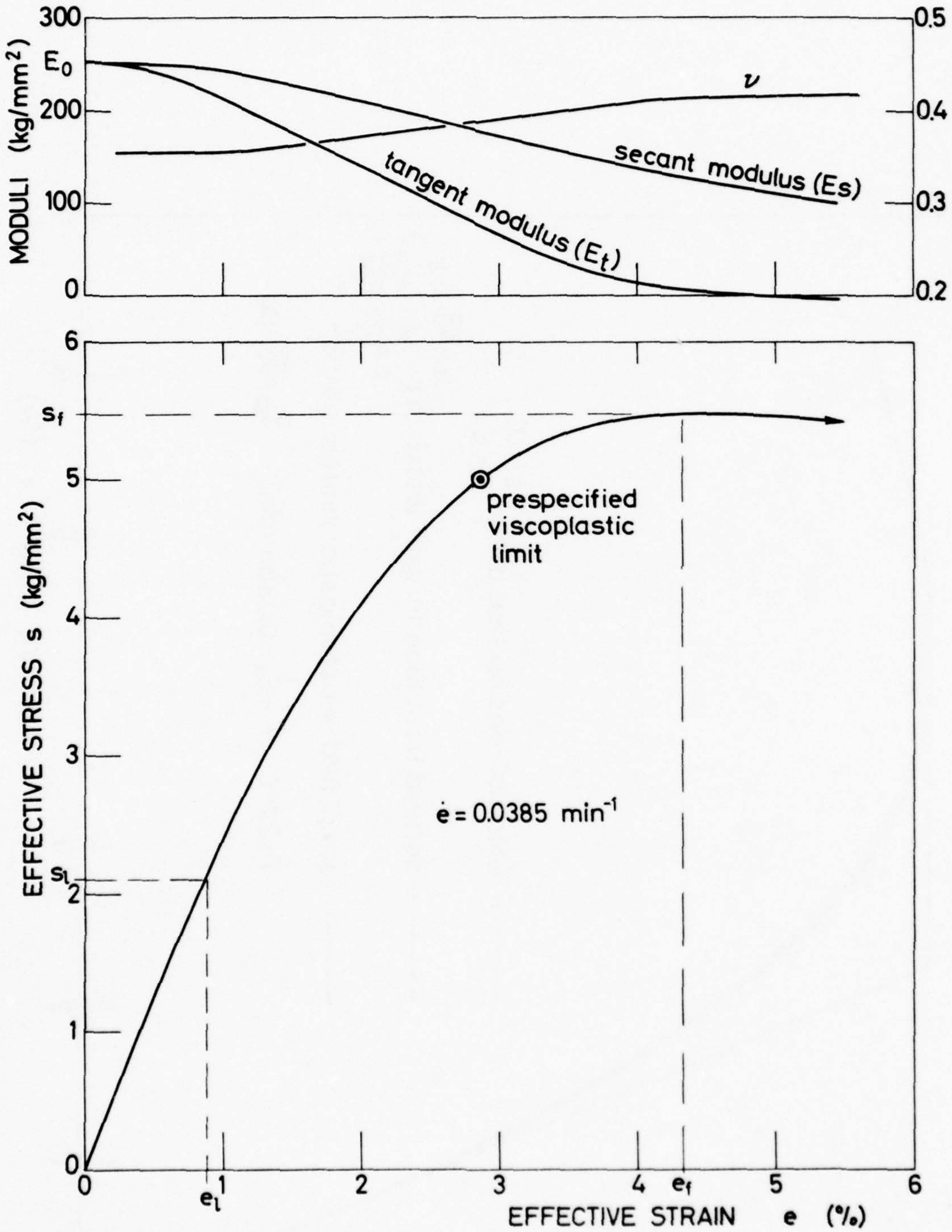

FIG. 8 THE EFFECT OF STRAIN ON THE VARIATION OF POISSON'S RATIO, TANGENT AND SECANT MODULI OF EPOXY RESIN USED FOR ADHESIVE LAYER.

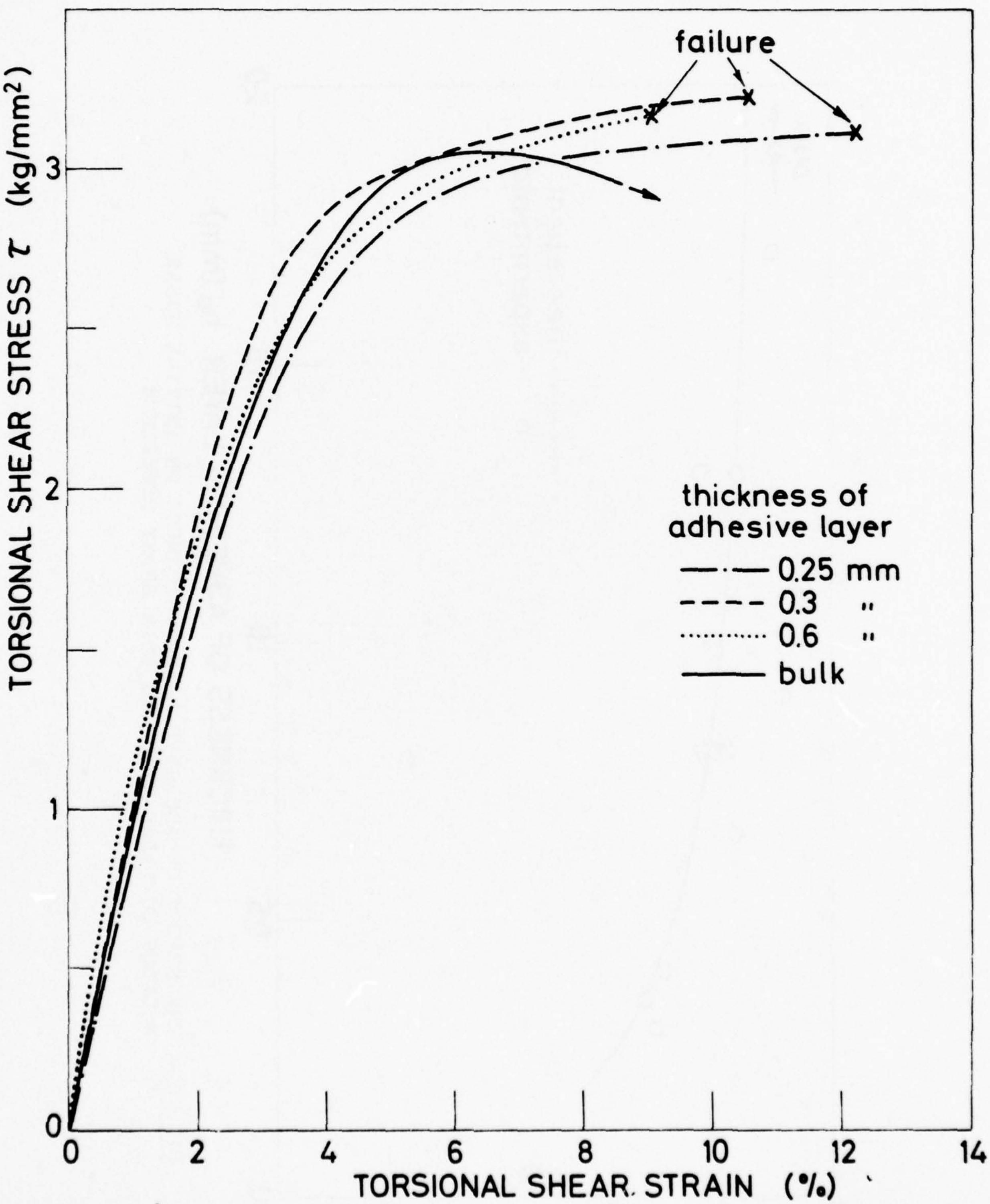

FIG. 9 TYPICAL SHEAR STRESS-STRAIN CURVES FOR THE ADHESIVE LAYER IN-SITU COMPARED WITH ITS BULK EPOXY REFERENCE (FIG. 6).

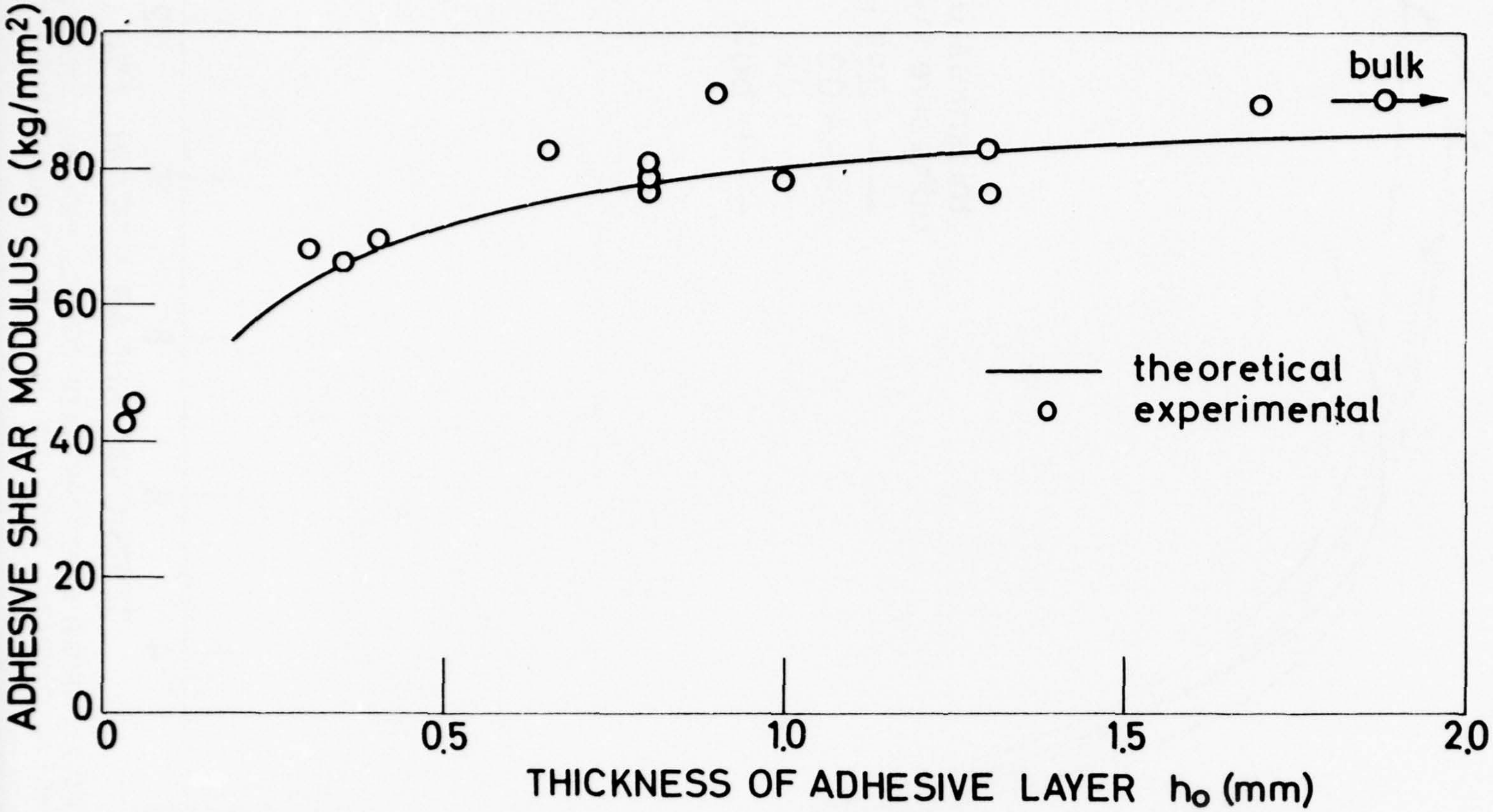

FIG. 10 THE EFFECT OF ADHESIVE LAYER THICKNESS ON INITIAL SHEAR MODULUS COMPARED WITH ITS BULK EPOXY REFERENCE.

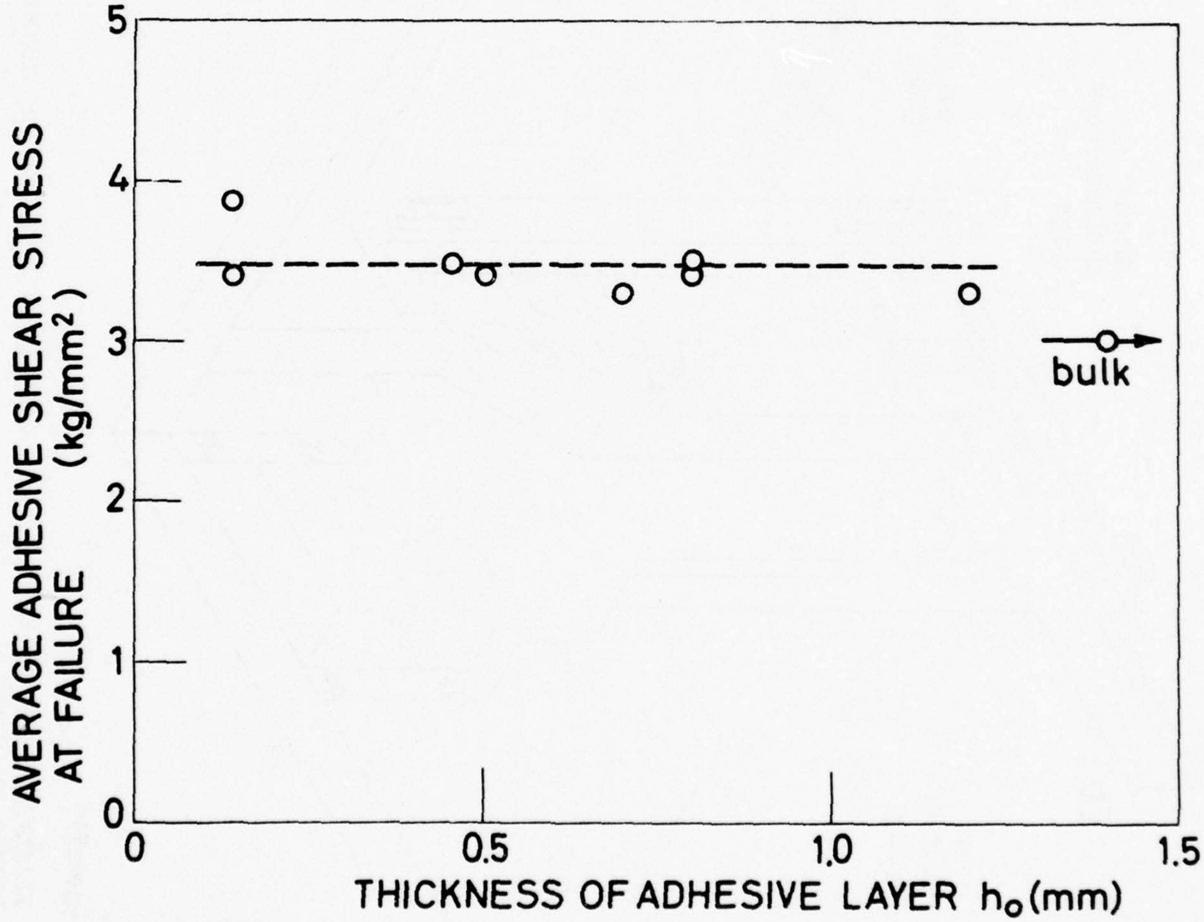

FIG. 11 THE EFFECT OF ADHESIVE LAYER THICKNESS ON ULTIMATE SHEAR STRENGTH COMPARED WITH ITS BULK EPOXY REFERENCE.

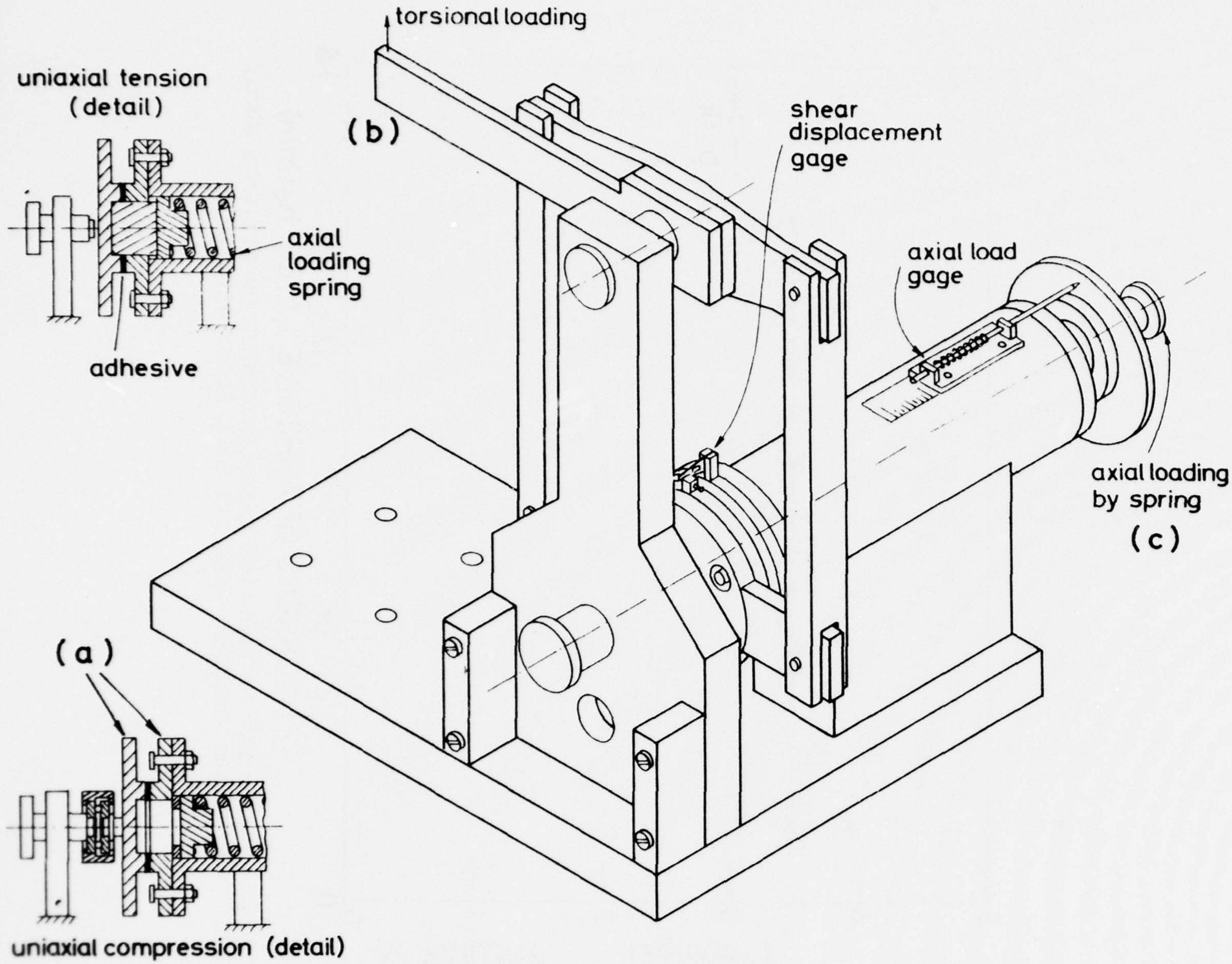

FIG. 12a ILLUSTRATION OF DEVICE FOR COMBINED LOADING OF ADHESIVE LAYER IN-SITU.

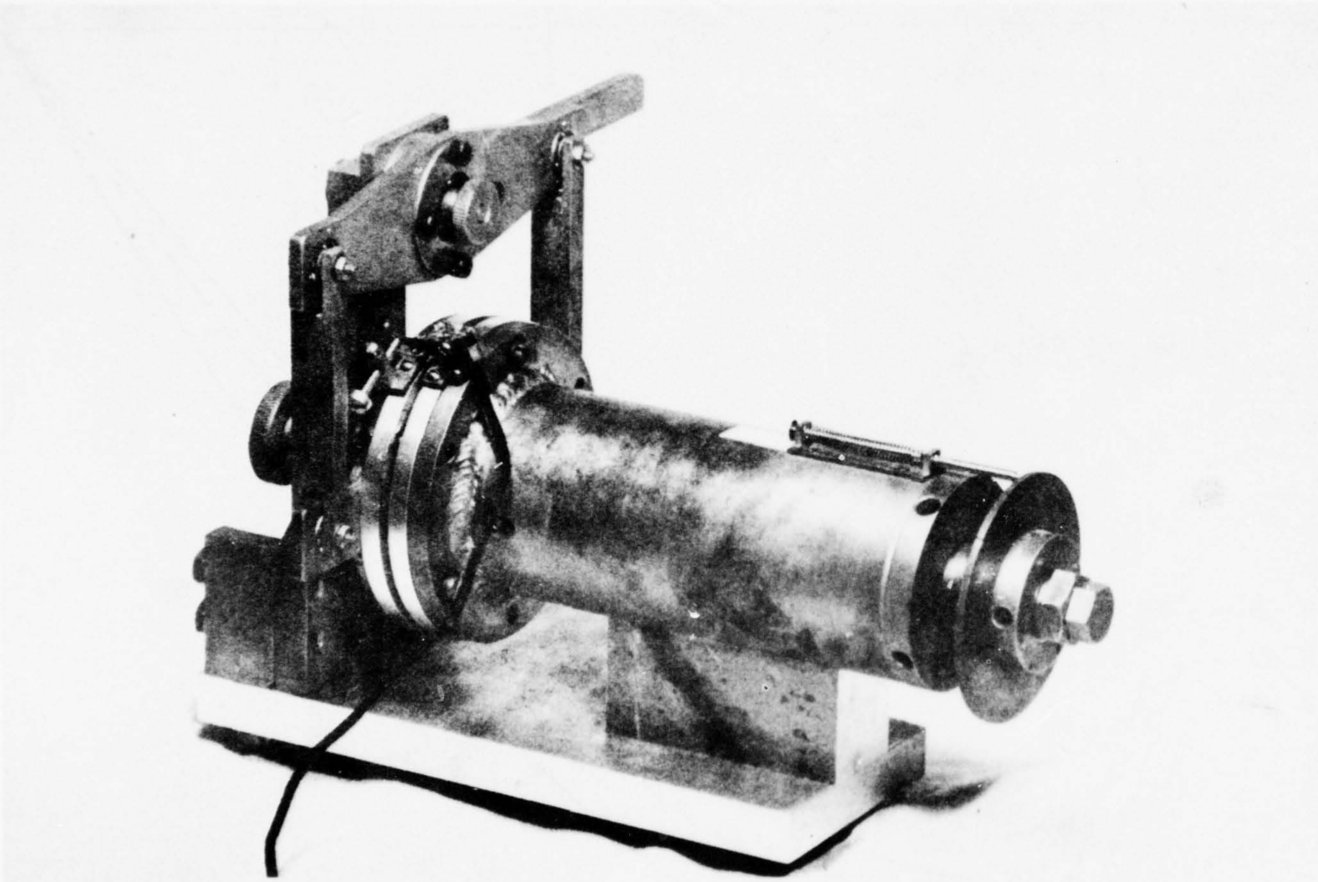

FIG. 12b PHOTOGRAPH OF DEVICE FOR COMBINED LOADING OF ADHESIVE LAYER IN-SITU.

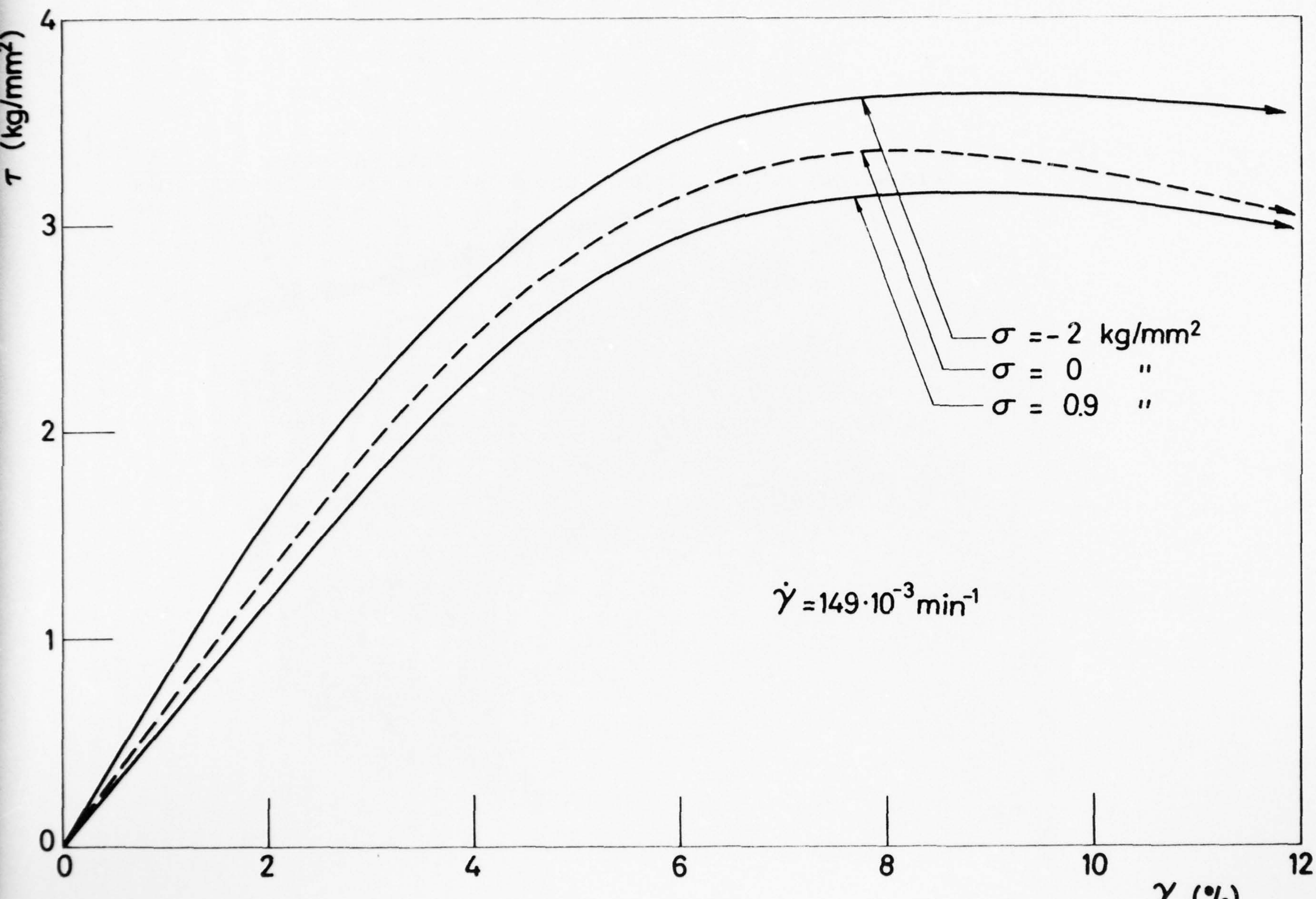

FIG. 13 TYPICAL SHEAR STRESS-STRAIN CURVES OF ADHESIVE LAYER IN-SITU UNDER COMBINED SHEAR AND AXIAL NORMAL LOADING.

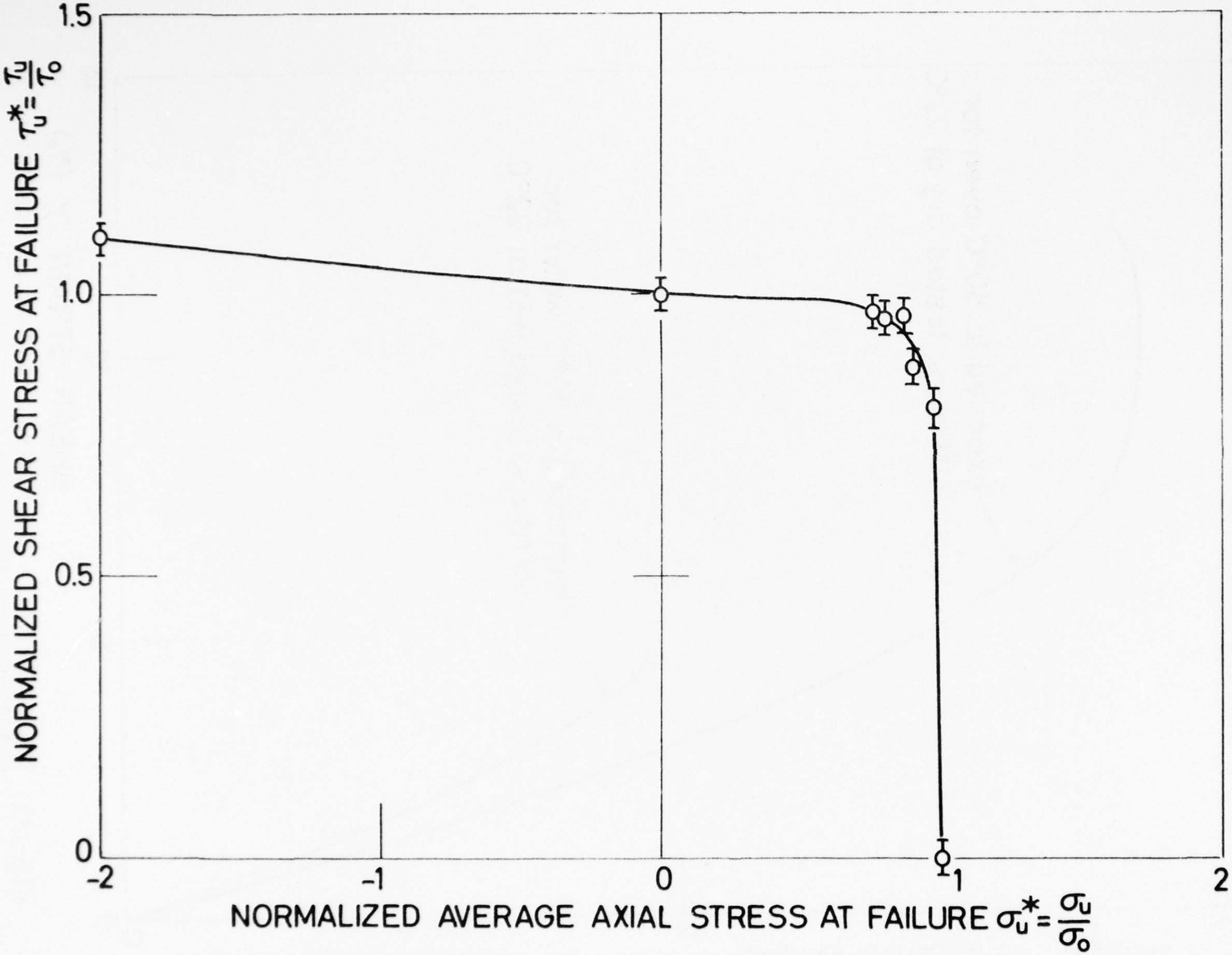

FIG. 14 FAILURE ENVELOPE FOR ADHESIVE LAYER IN-SITU (LOADED UNDER COMBINED SHEAR AND AXIAL NORMAL STRESS).

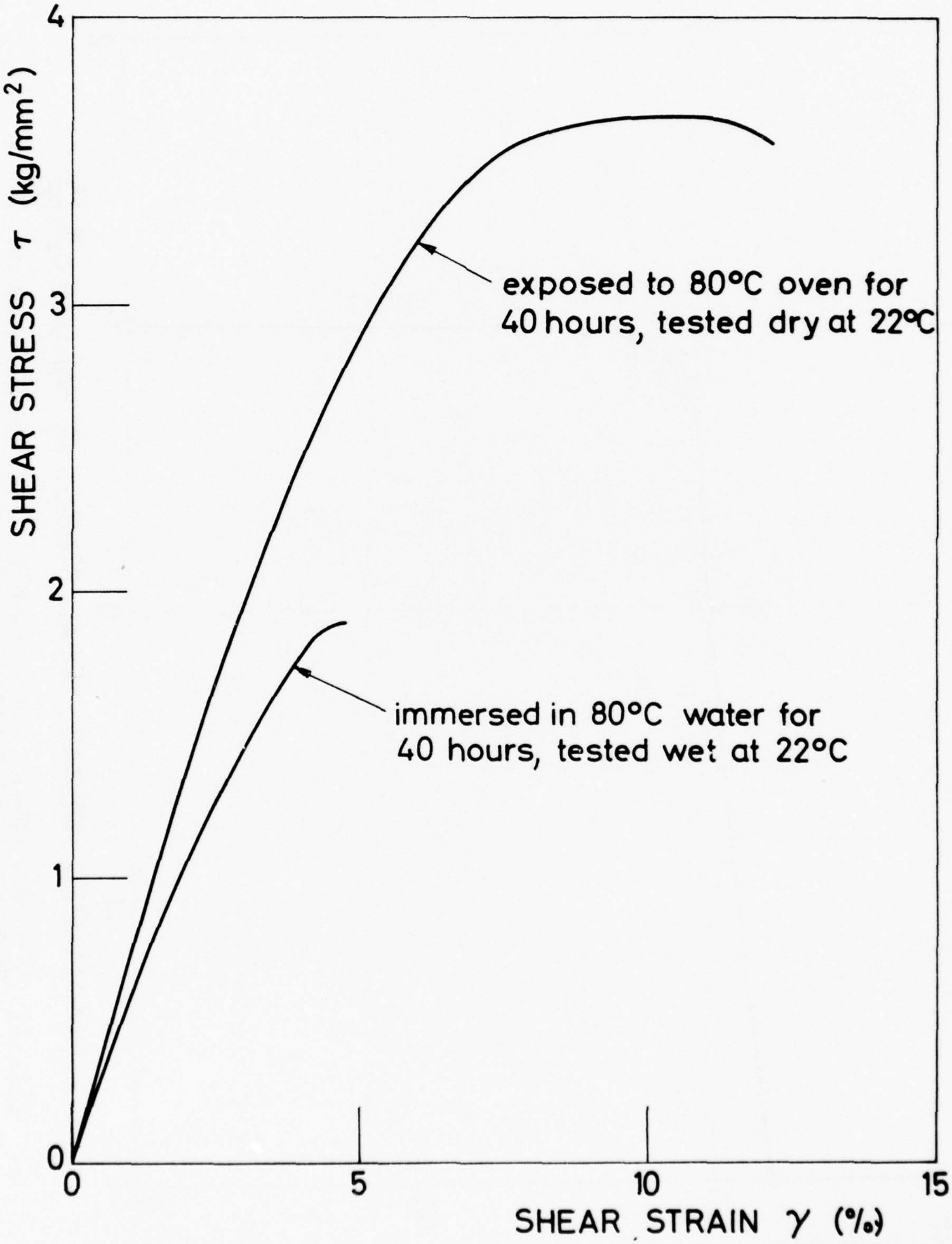

FIG. 15 THE EFFECT OF HYGROTHERMAL HISTORY ON ADHESIVE STRESS-STRAIN BEHAVIOR.

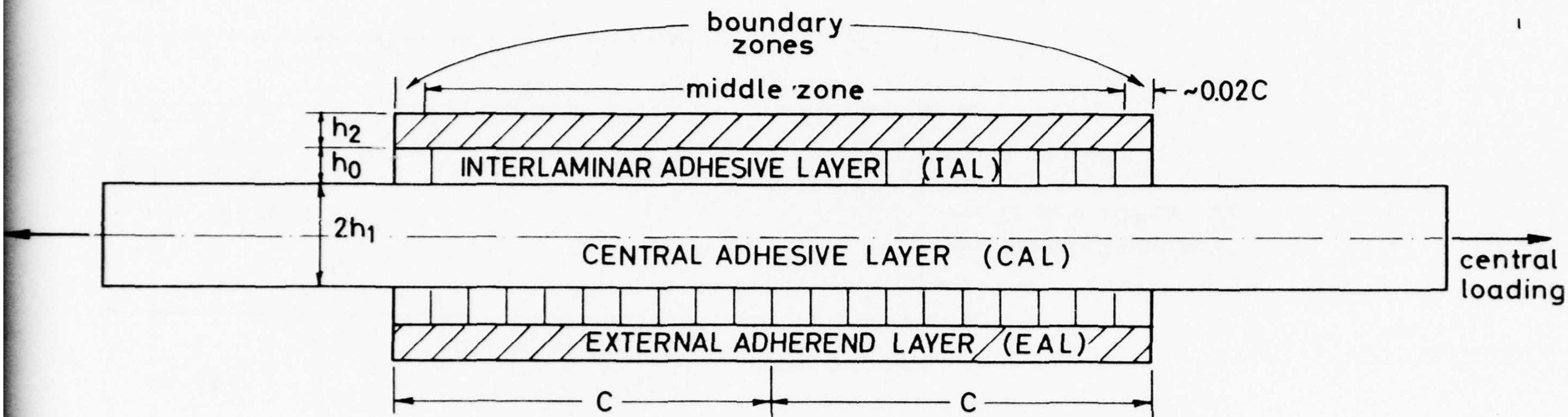

FIG. 16 SYMMETRICAL DOUBLER MODEL.

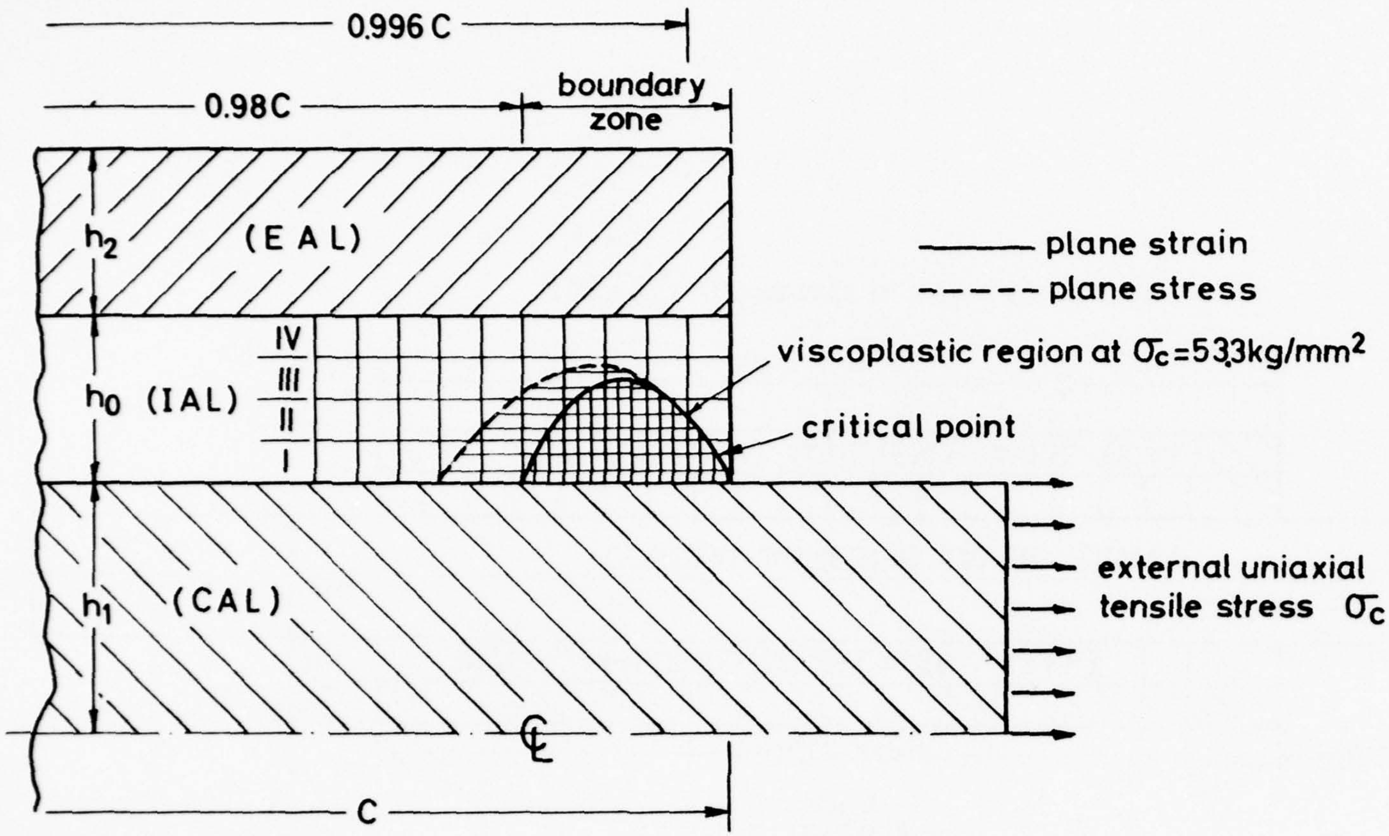

FIG. 17 ILLUSTRATION OF IAL NETWORK AT THE BOUNDARY ZONE USED FOR FINITE ELEMENT NON-LINEAR STRESS ANALYSIS.

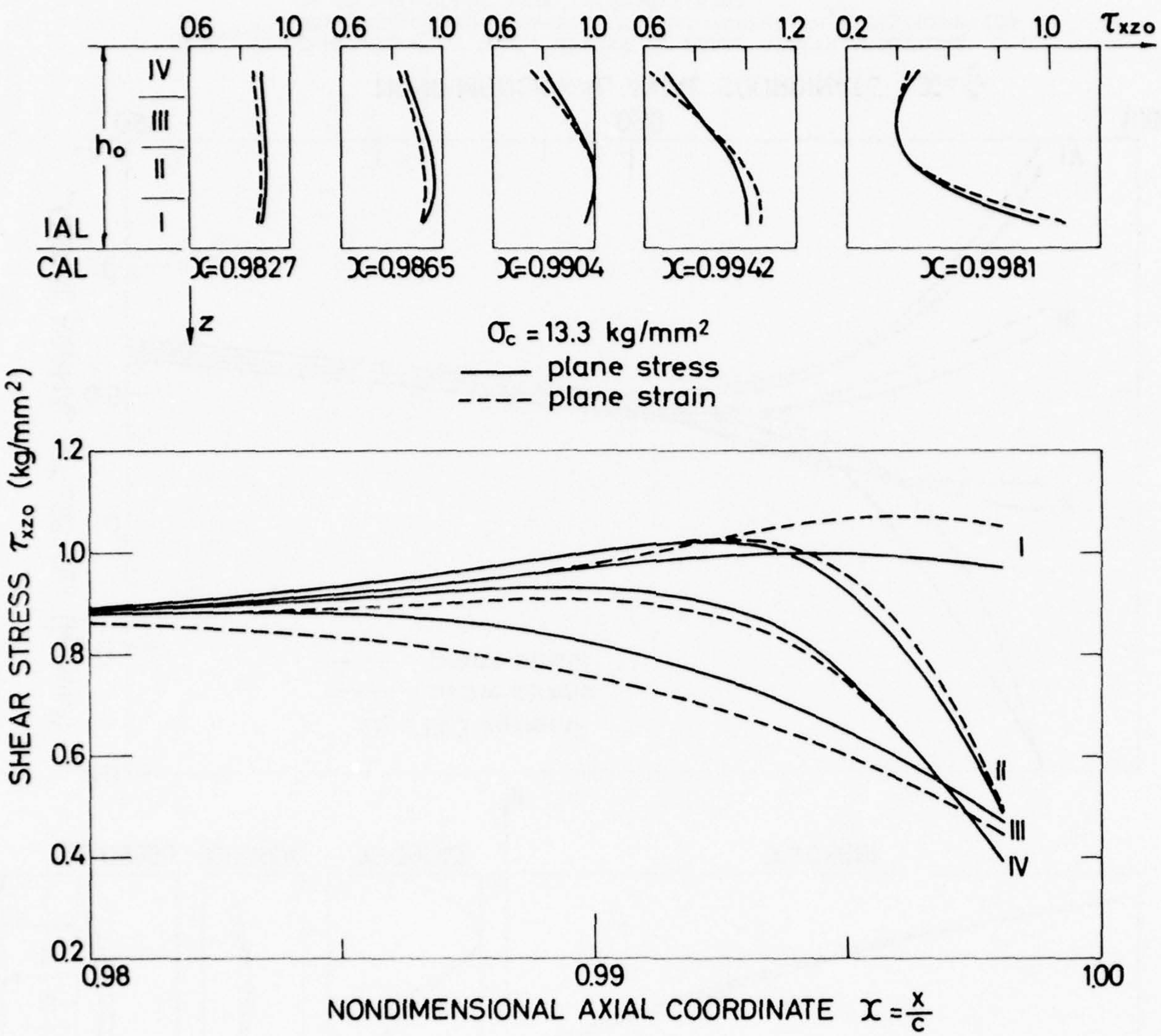

FIG. 18 COMPARISON OF PLANE STRESS VS PLANE STRAIN SOLUTIONS FOR INTERLAMINAR SHEAR-STRESS (τ_{xz}) DISTRIBUTION AT THE BOUNDARY ZONE (LINEAR RANGE).

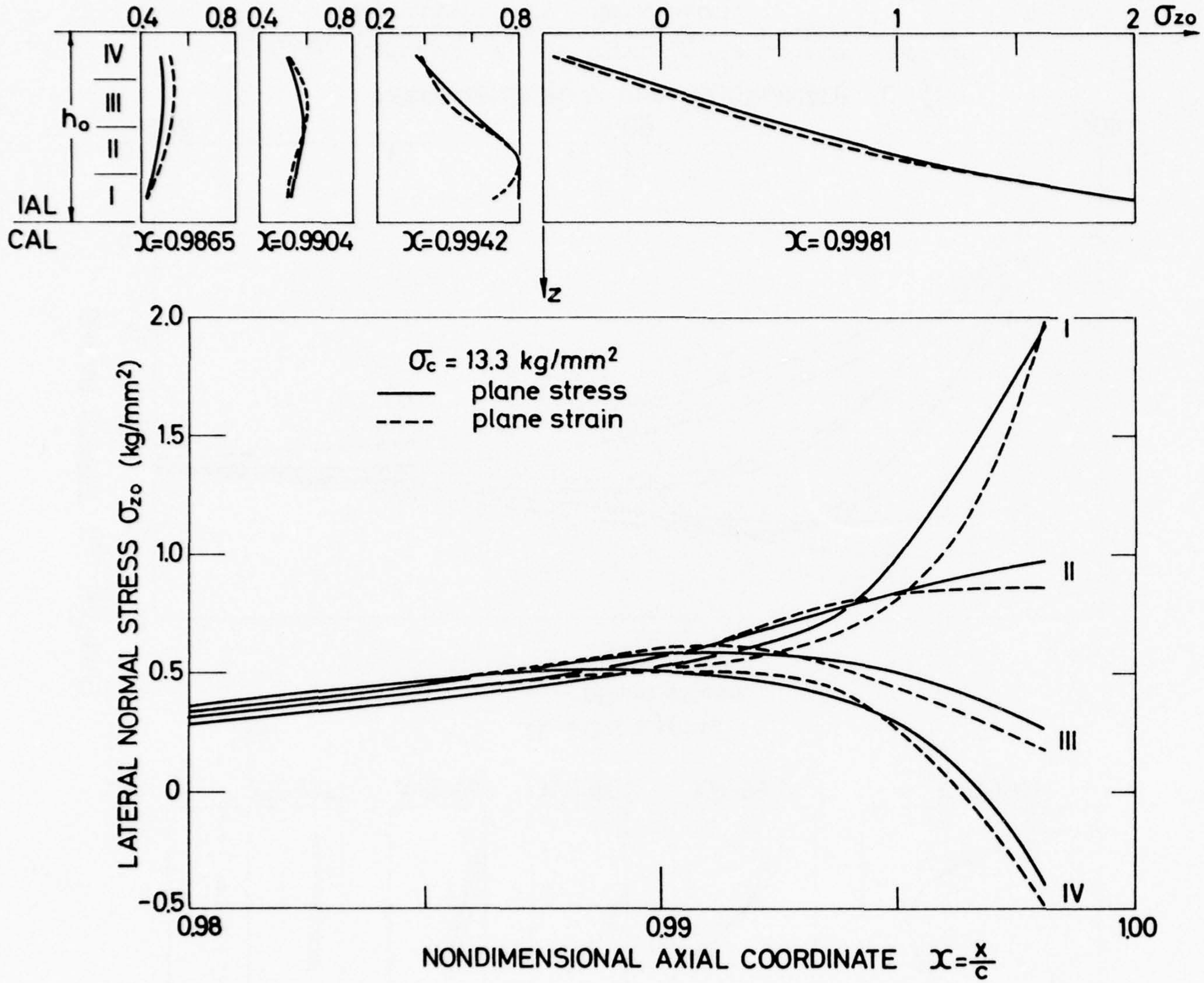

FIG. 19 COMPARISON OF PLANE STRESS VS PLANE STRAIN SOLUTIONS FOR INTERLAMINAR LATERAL NORMAL STRESS (σ_z) DISTRIBUTION AT THE BOUNDARY ZONE (LINEAR RANGE).

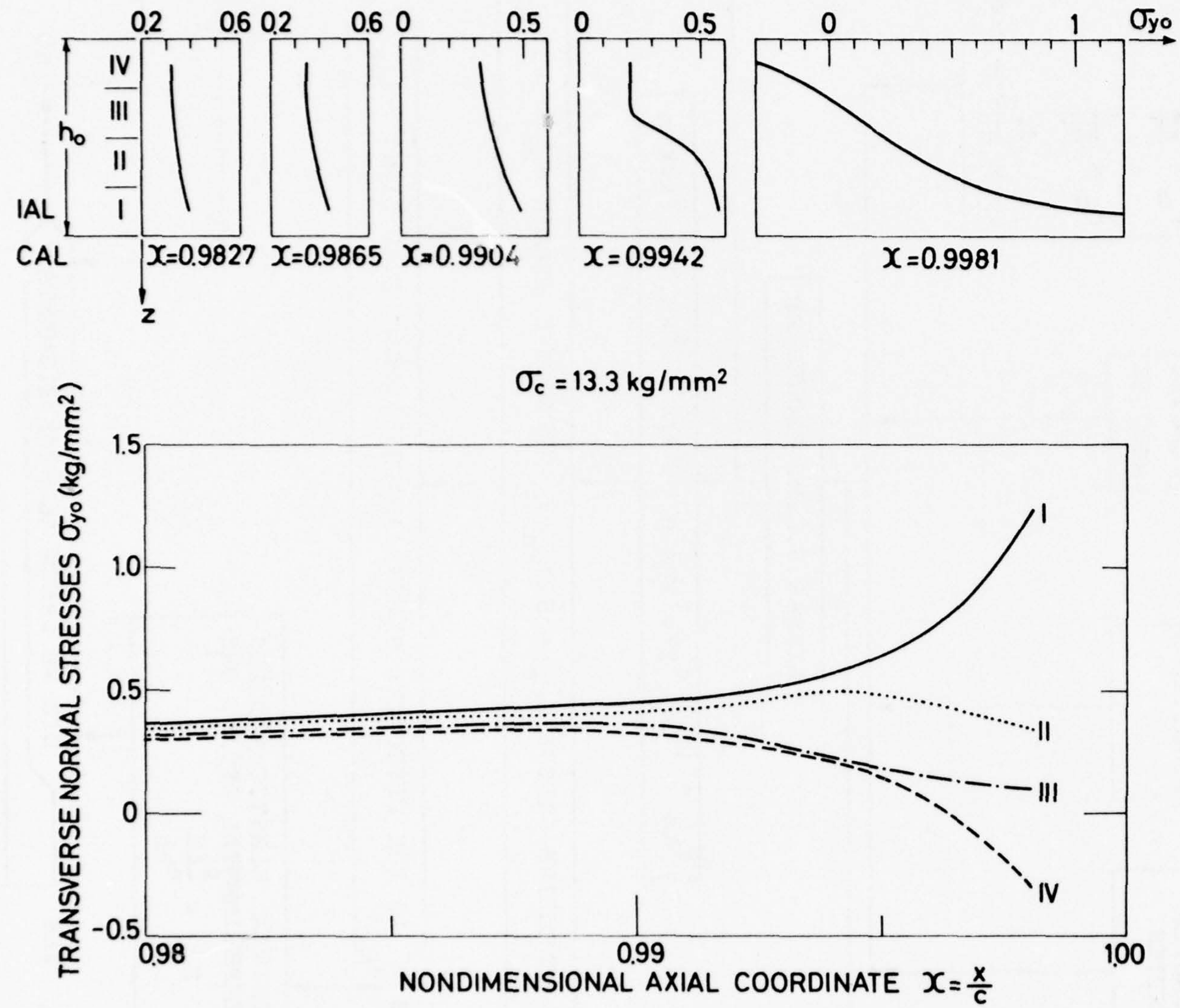

FIG. 20 PLANE STRAIN SOLUTION FOR INTERLAMINAR TRANSVERSE NORMAL STRESS (σ_y) DISTRIBUTION AT THE BOUNDARY ZONE.

FLOW CHART

FOR STRESS ANALYSIS OF INTERLAMINAR ADHESIVE LAYER
AT THE NONLINEAR RANGE.

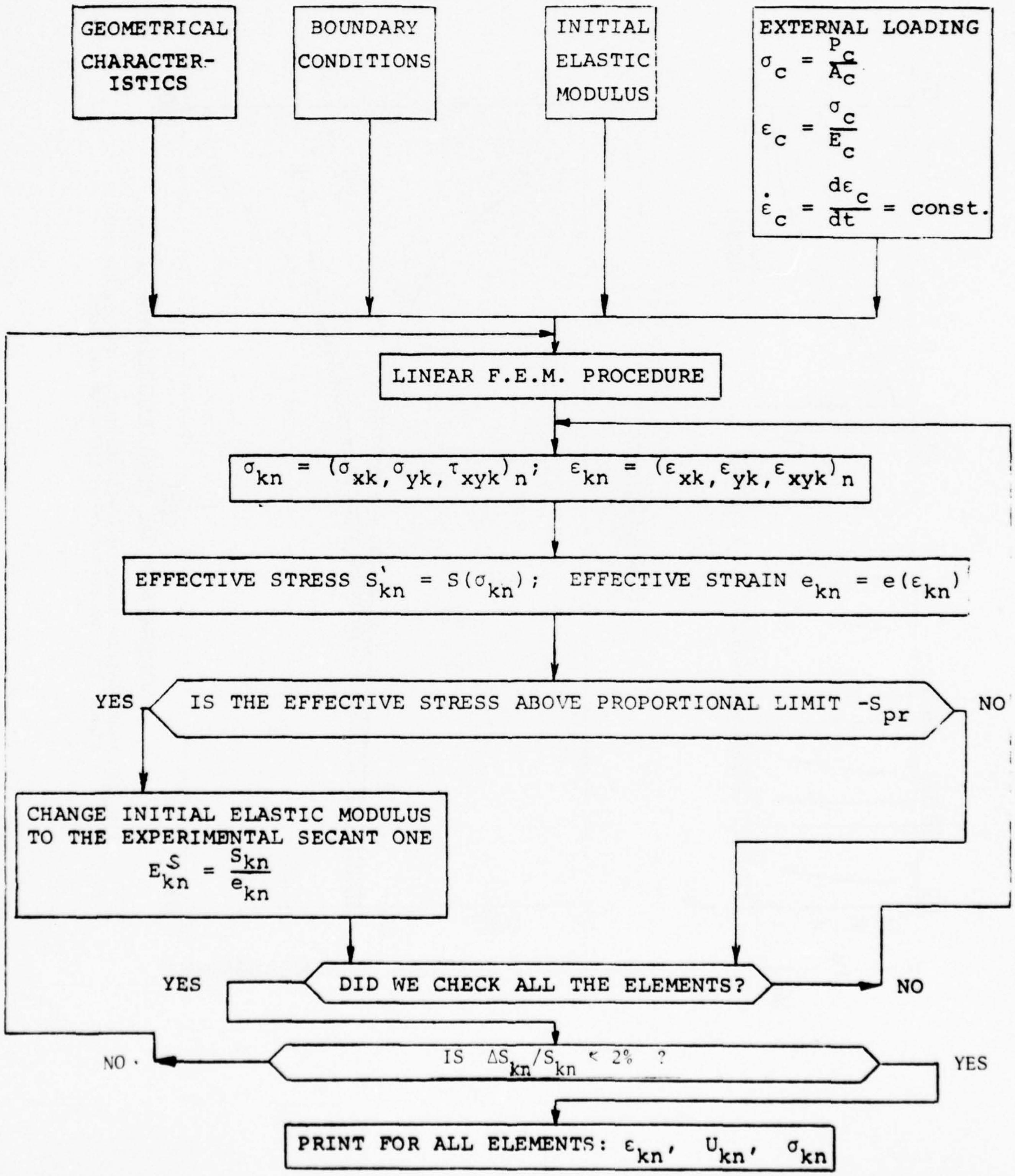

FIG. 21 FLOW CHART FOR STRESS ANALYSIS OF INTERLAMINAR ADHESIVE LAYER AT THE NON-LINEAR RANGE.

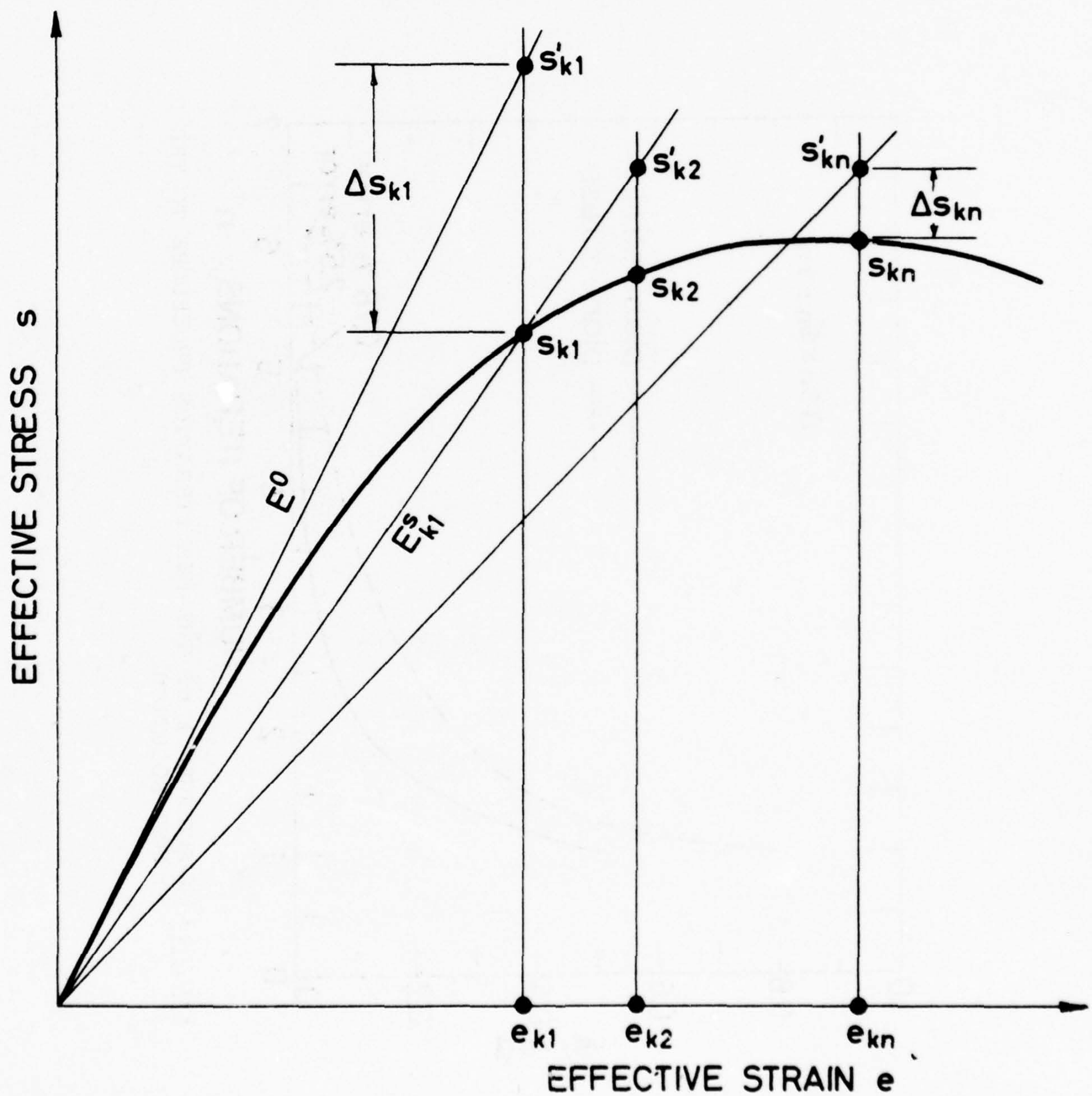

FIG. 22 ILLUSTRATION OF FEM PROCEDURE FOR STRESS ANALYSIS OF TAL AT THE NONLINEAR RANGE.

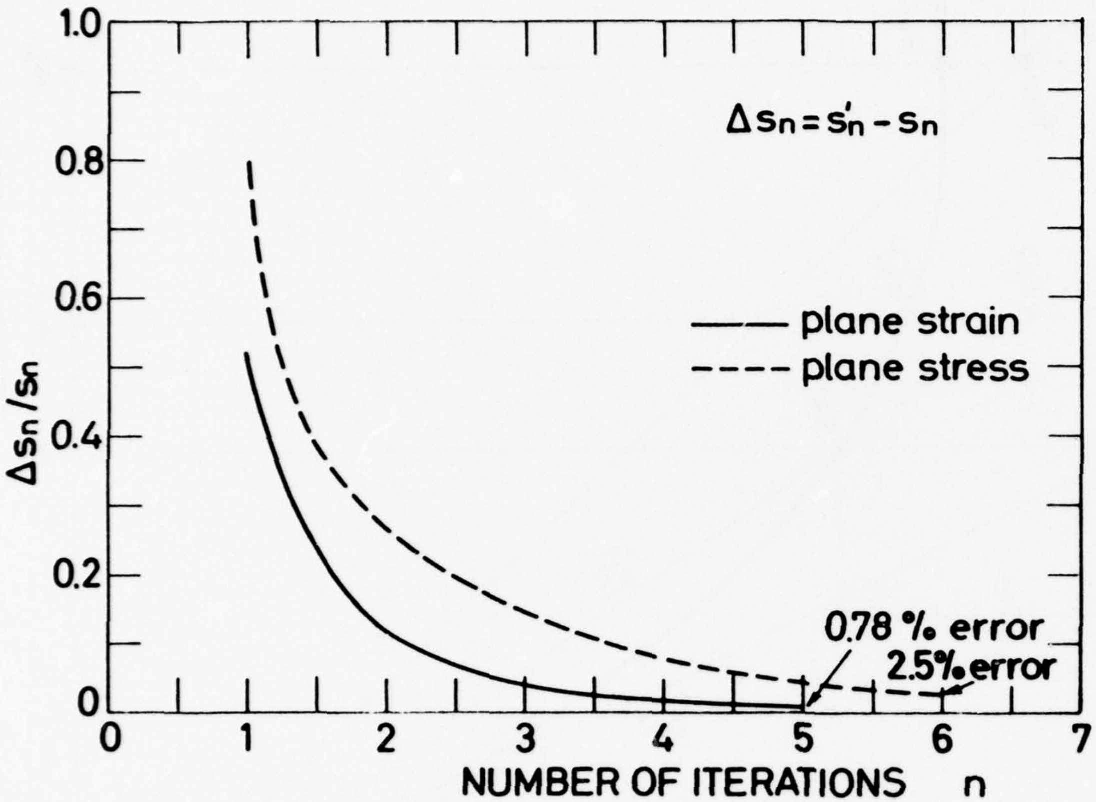

FIG. 23 CONVERGENCE OF THE FEM ITERATION PROCEDURE TO THE EXACT SOLUTION.

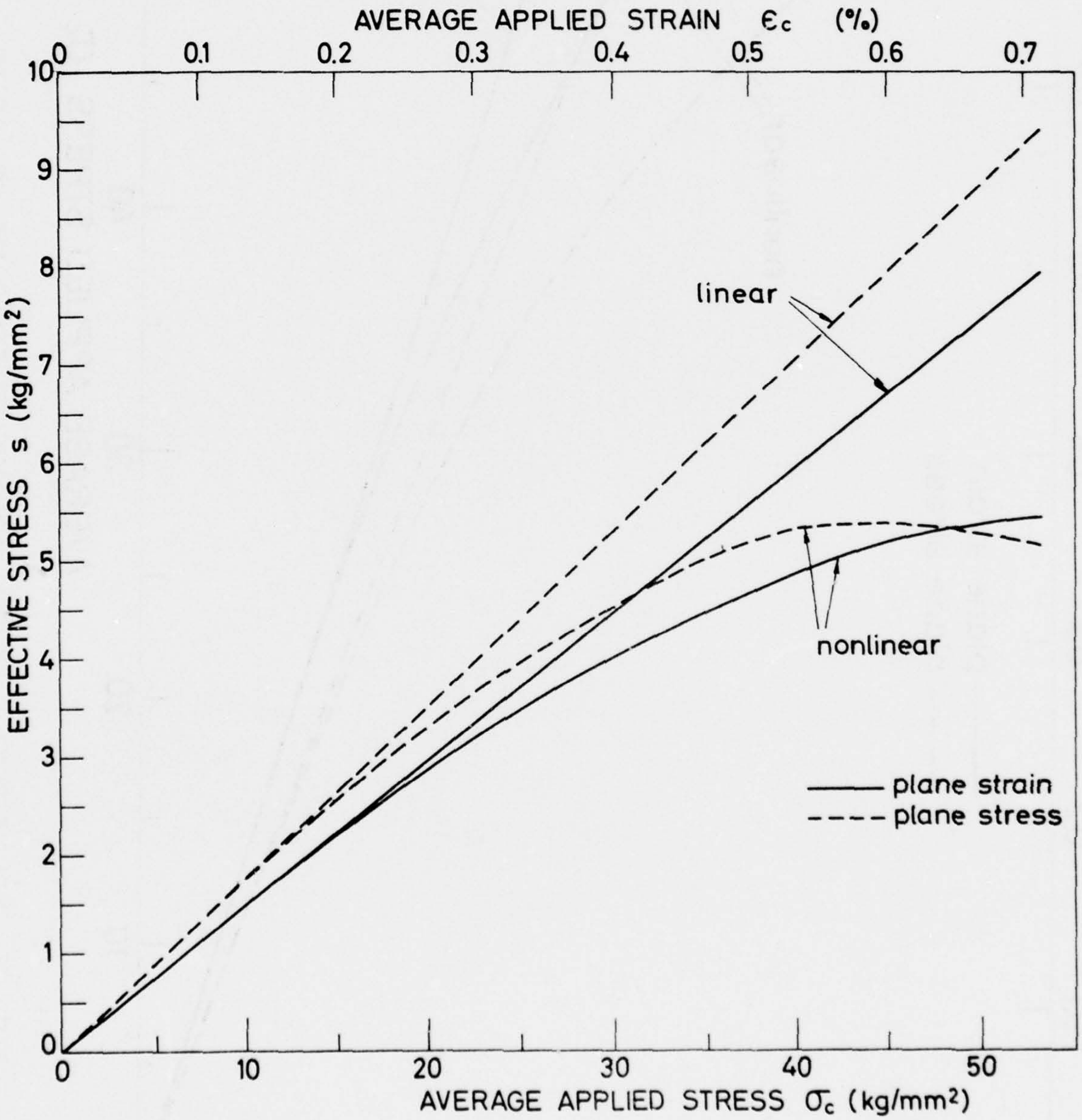

FIG. 24 THE EFFECT OF CENTRAL LOADING ON EFFECTIVE STRESSES AT THE CRITICAL POINTS IN THE BOUNDARY ZONE OF THE IAL.

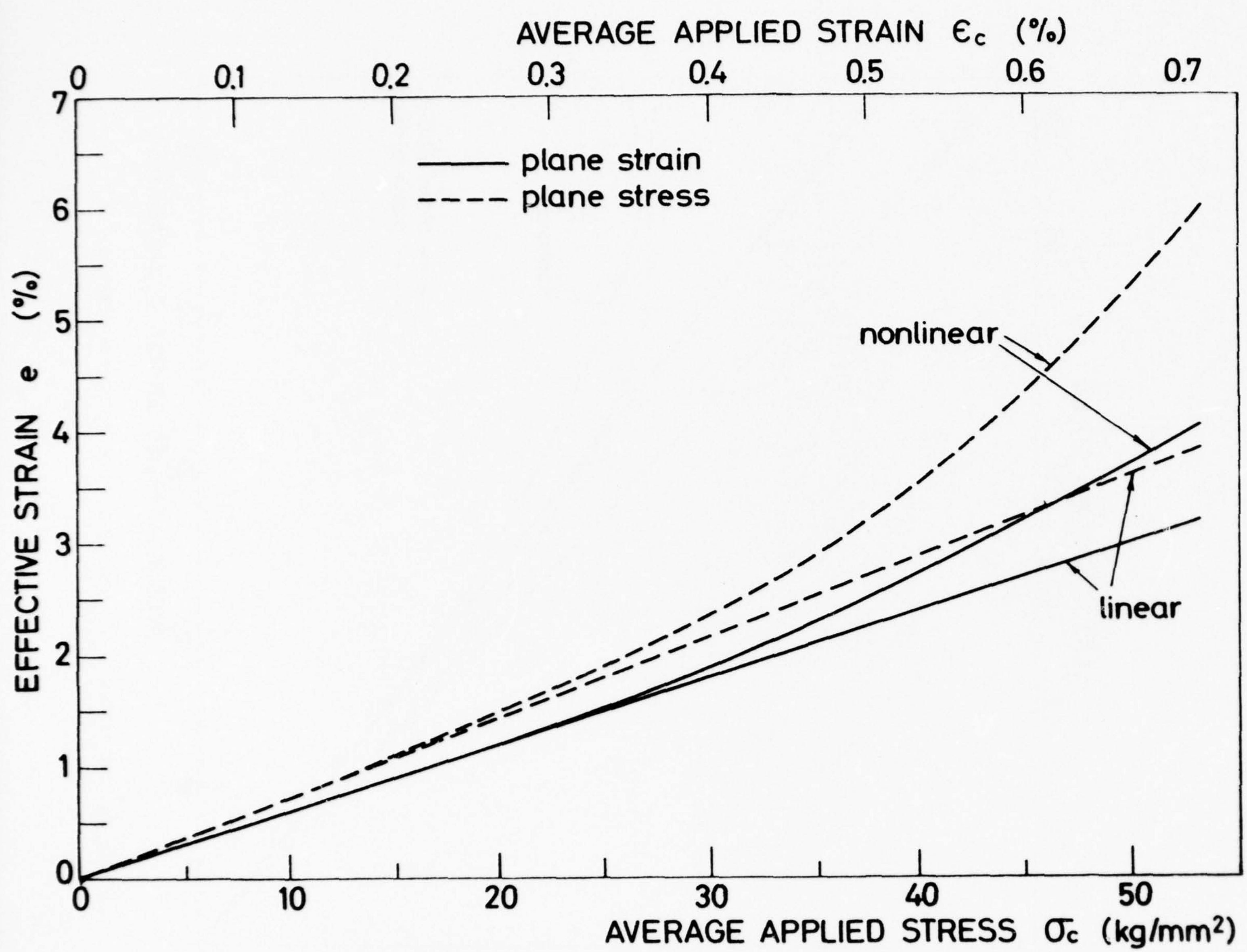

FIG. 25 THE EFFECT OF CENTRAL LOADING ON EFFECTIVE STRAIN AT THE CRITICAL POINTS IN THE BOUNDARY ZONE OF THE IAL.

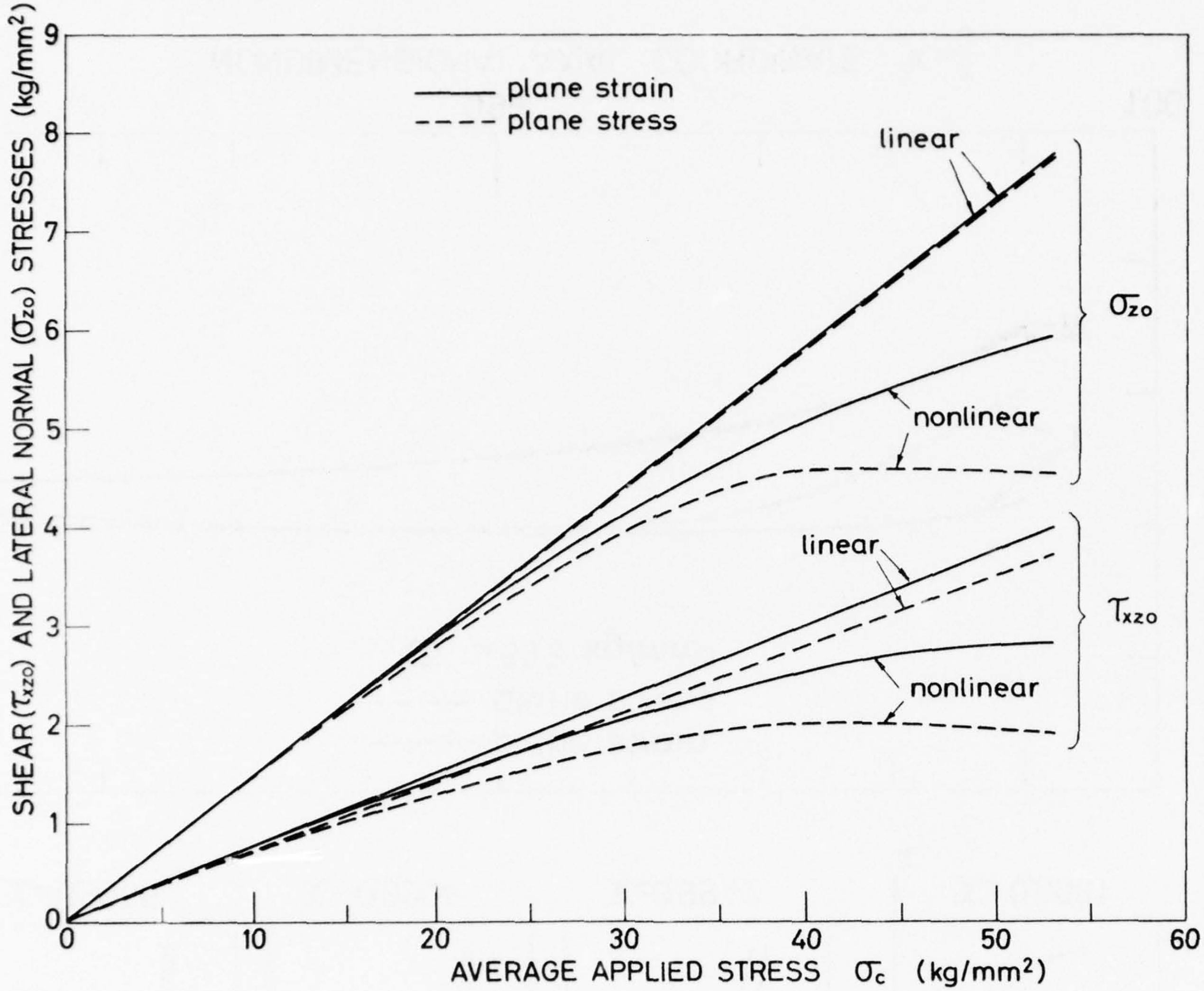

FIG. 26 THE EFFECT OF CENTRAL LOADING ON SHEAR AND NORMAL STRESSES AT THE CRITICAL POINT IN THE BOUNDARY ZONE OF THE IAL.

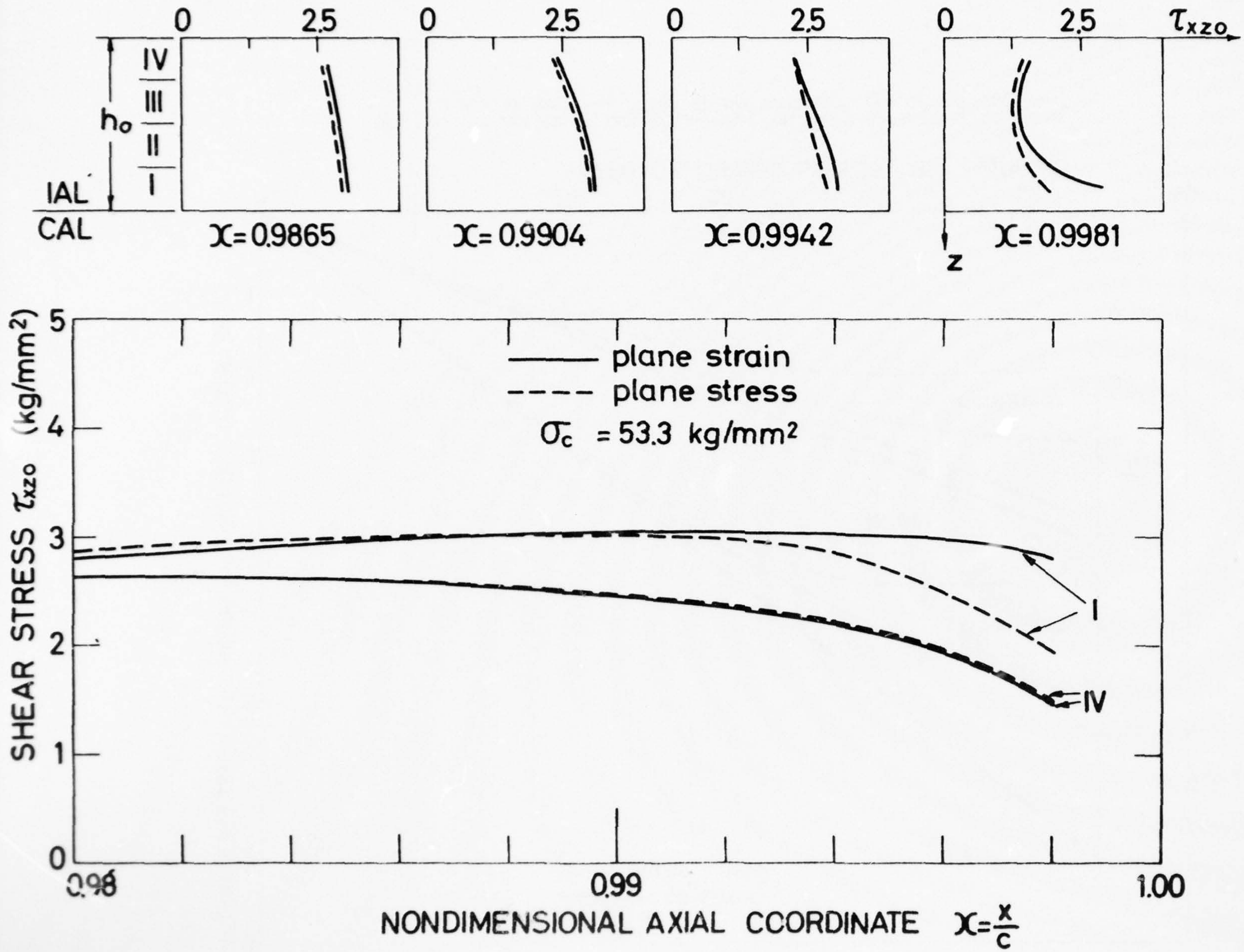

FIG. 27 SHEAR STRESS DISTRIBUTION AT THE BOUNDARY ZONE OF THE IAL (NON-LINEAR RANGE).

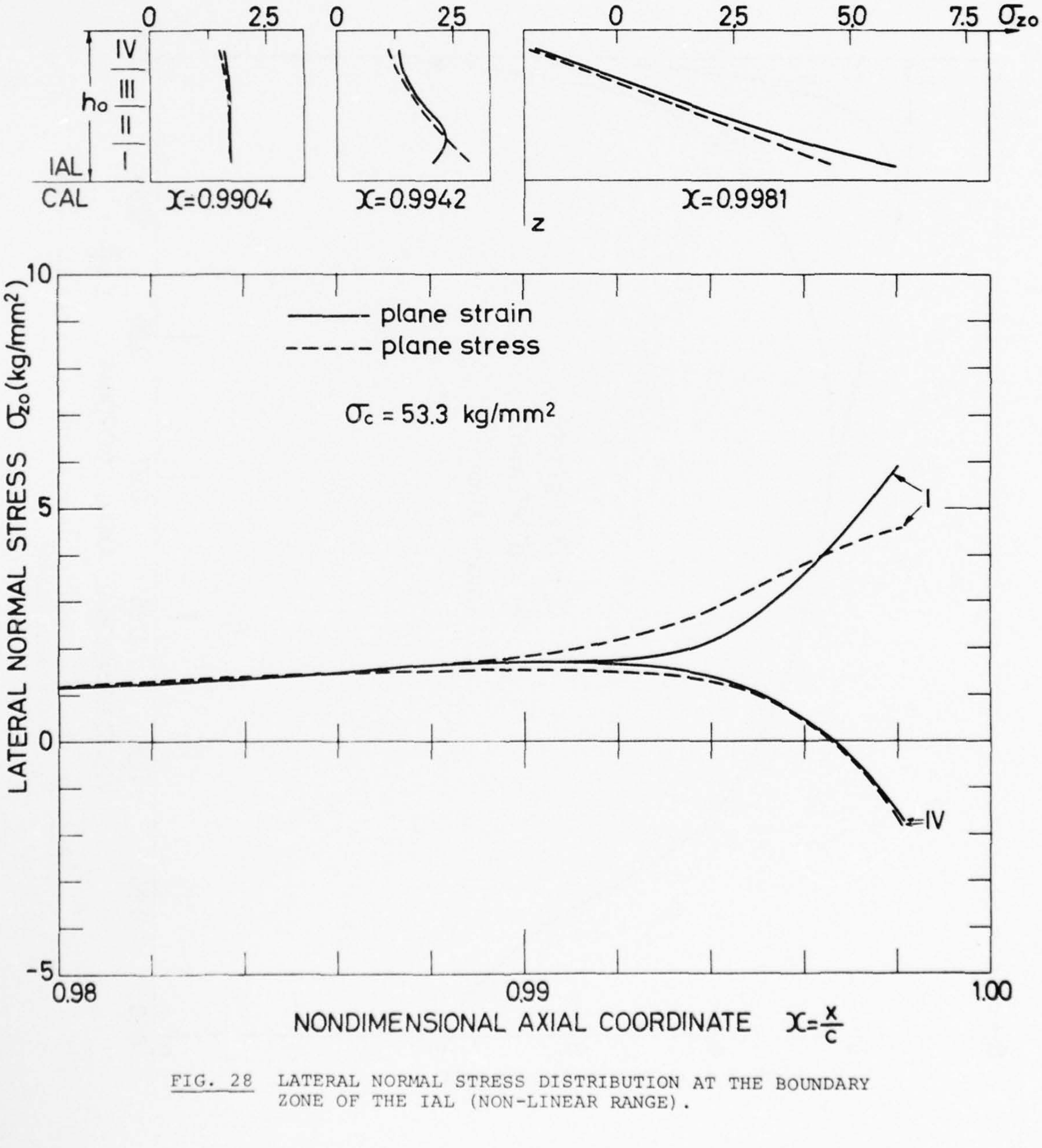

FIG. 28 LATERAL NORMAL STRESS DISTRIBUTION AT THE BOUNDARY ZONE OF THE IAL (NON-LINEAR RANGE).

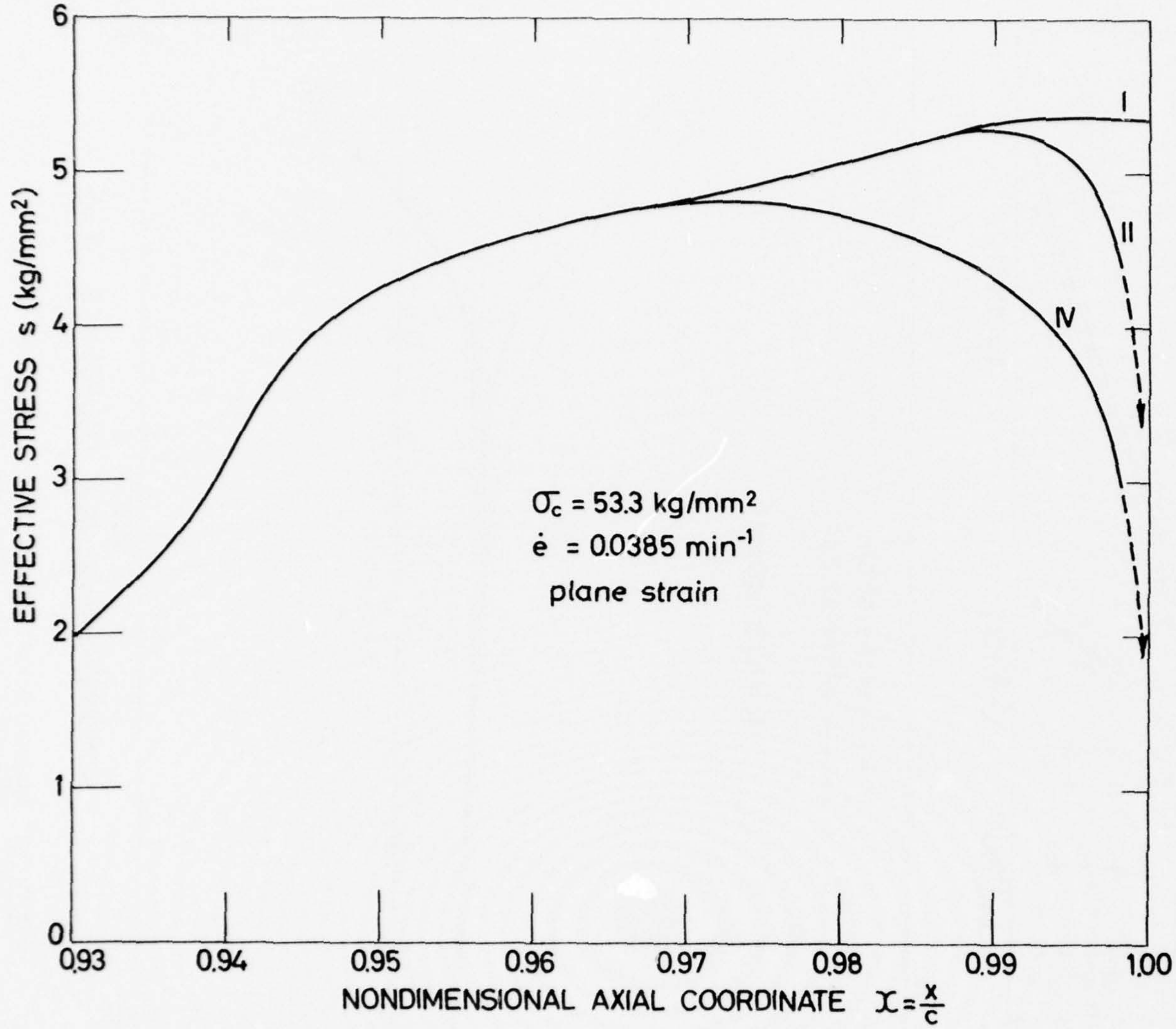

FIG. 29 EFFECTIVE STRESS DISTRIBUTION ALONG THE IAL (NON-LINEAR RANGE).

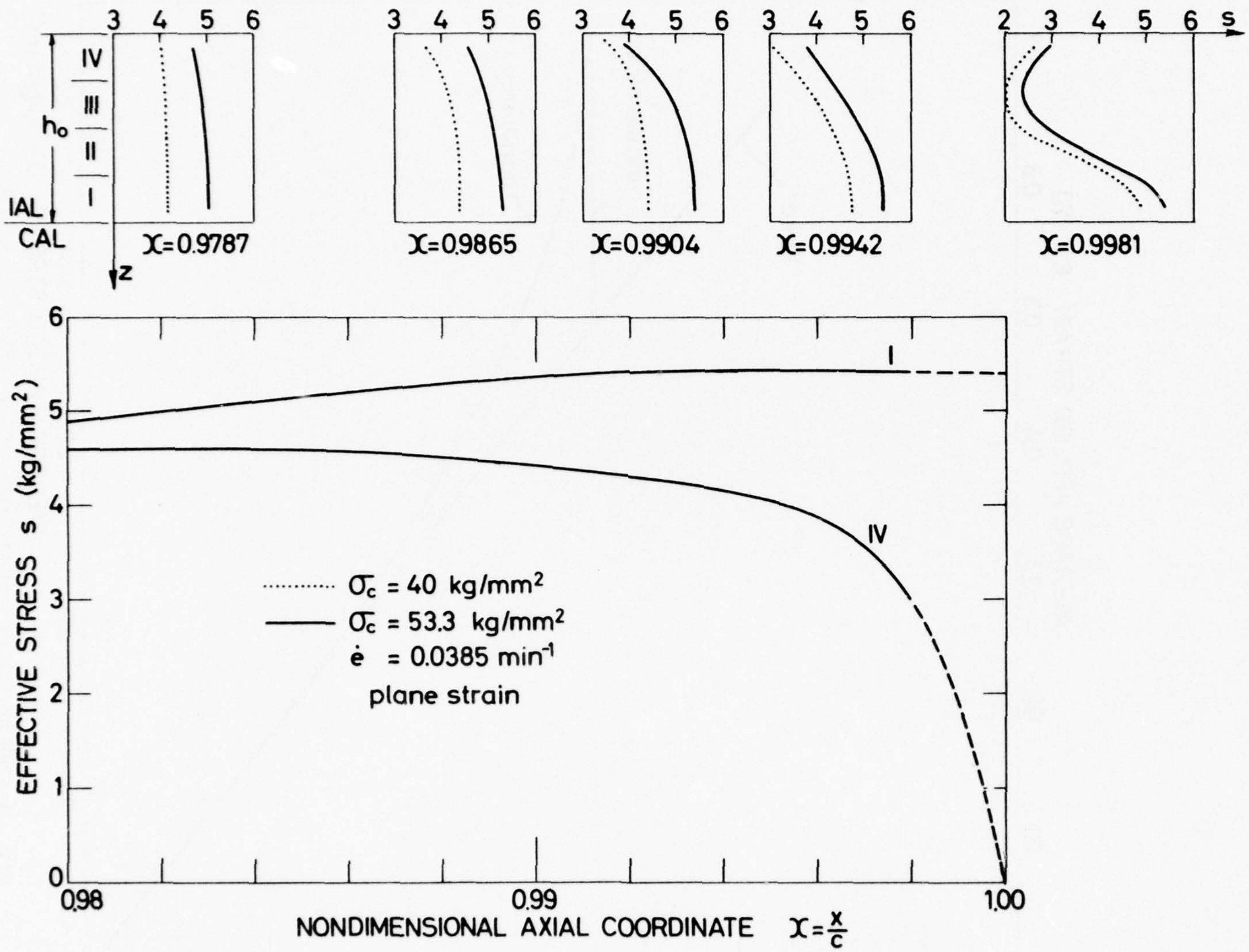

FIG. 30 EFFECTIVE STRESS DISTRIBUTION AT THE IAL BOUNDARY ZONE (NON-LINEAR RANGE).

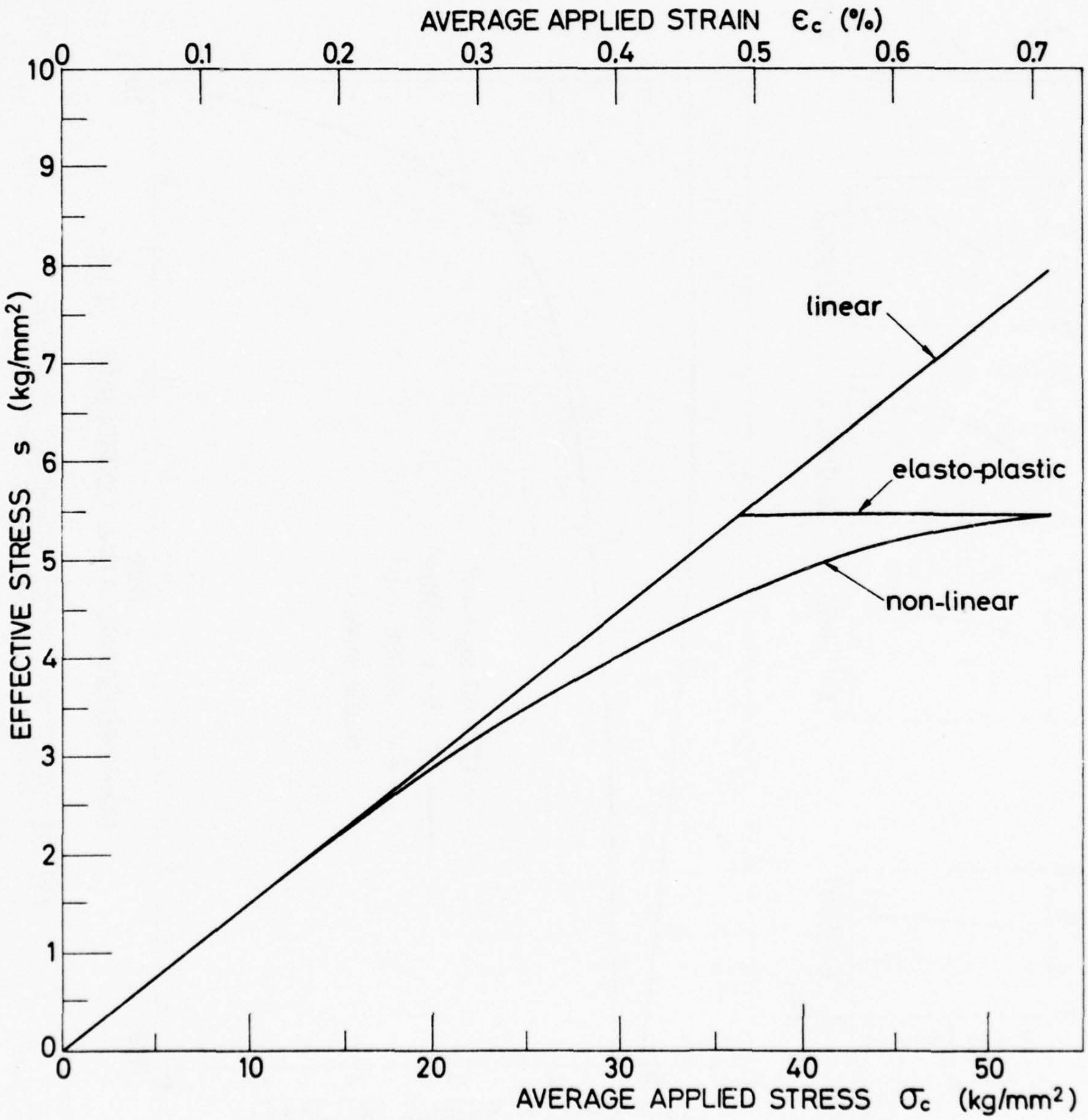

FIG. 31 THE EFFECT OF CENTRAL LOADING ON EFFECTIVE STRESSES AT THE CRITICAL POINT IN THE BOUNDARY ZONE OF THE IAL (PLANE STRAIN, SIMPLIFIED ELASTO-PLASTIC VS NON-LINEAR SOLUTIONS).

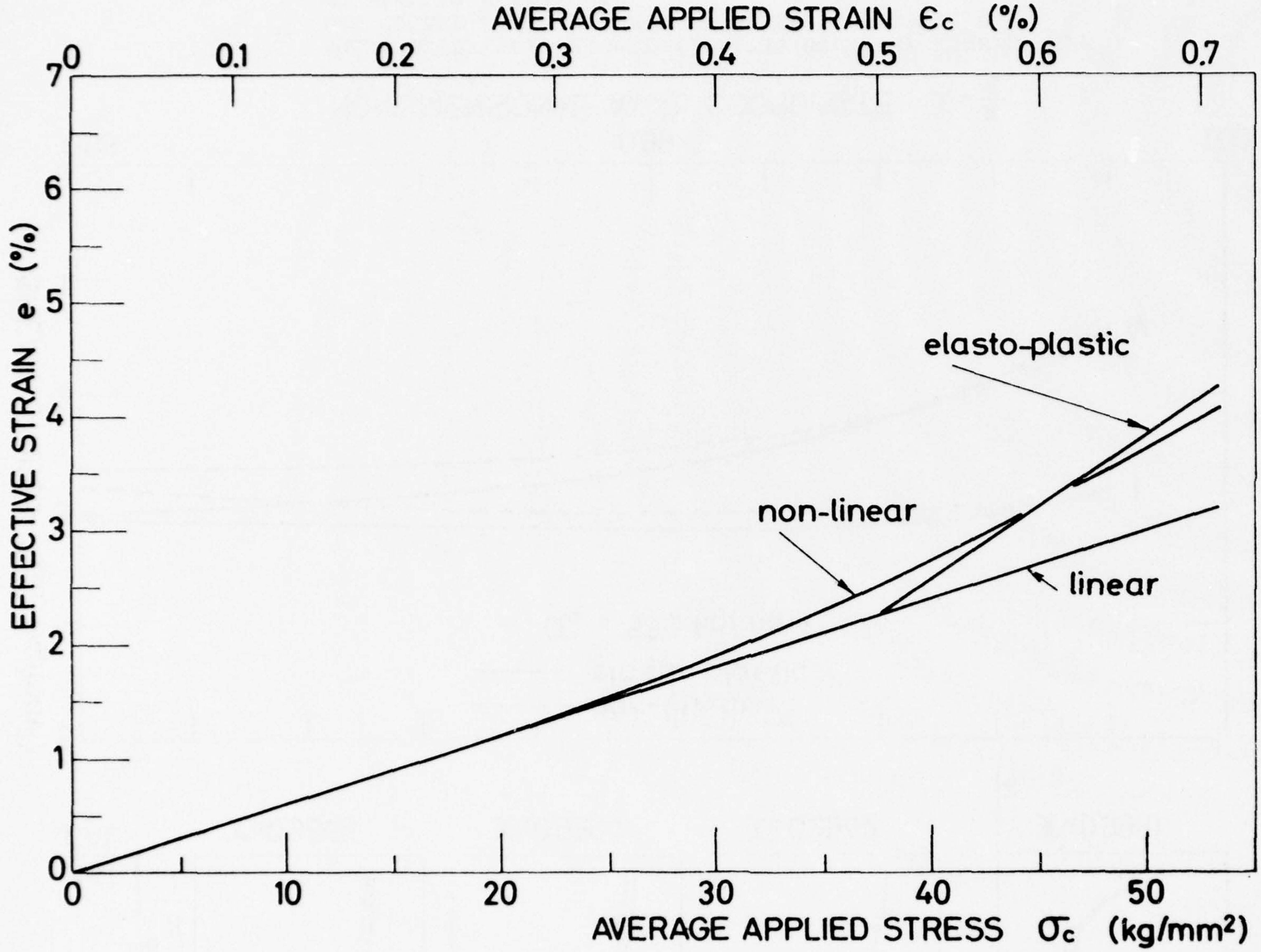

FIG. 32 THE EFFECT OF CENTRAL LOADING ON EFFECTIVE STRAINS AT THE CRITICAL POINT IN THE BOUNDARY ZONE OF THE IAL (PLANE STRAIN, SIMPLIFIED ELASTO-PLASTIC VS NON-LINEAR SOLUTIONS).

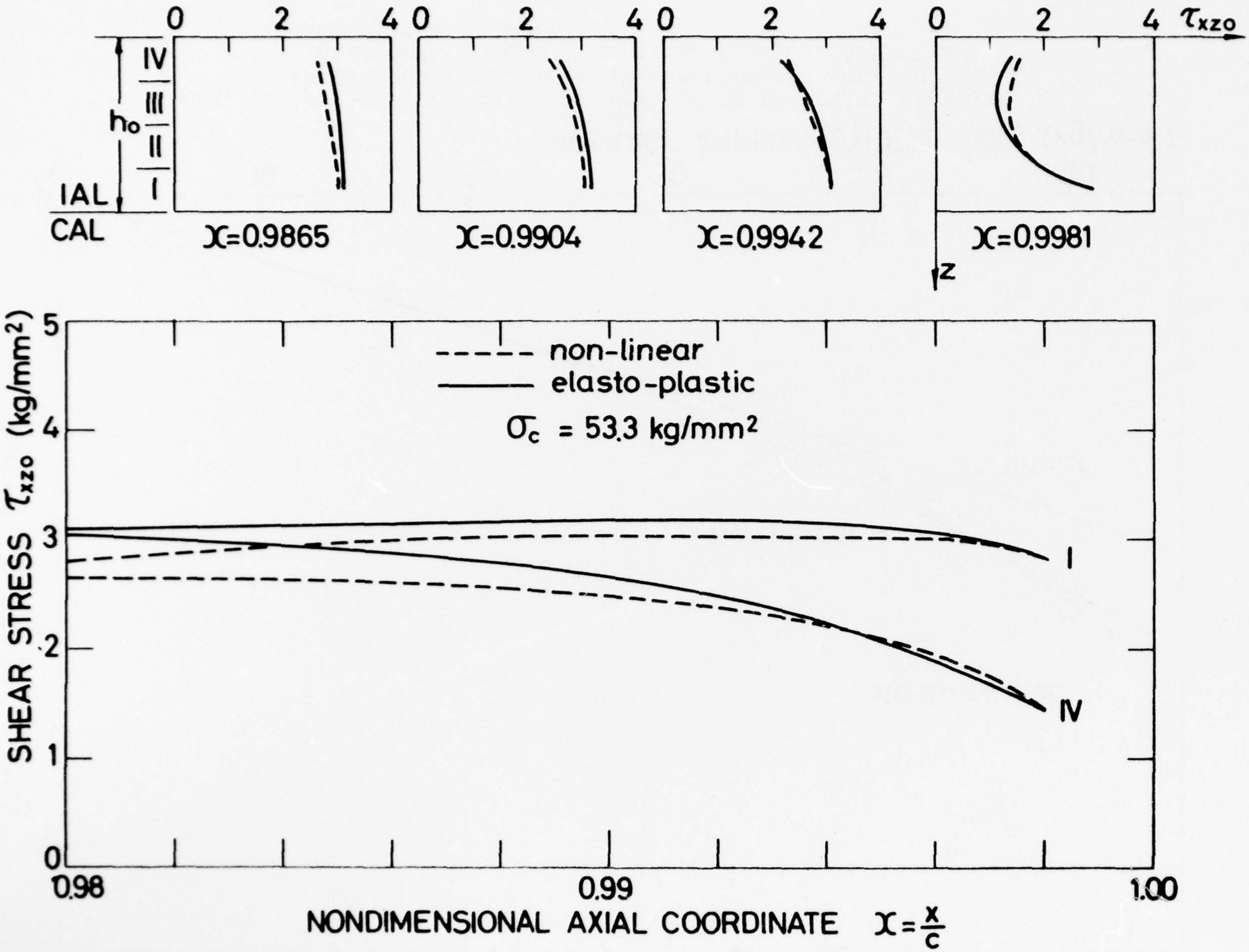

FIG. 33 SHEAR STRESS DISTRIBUTION AT THE BOUNDARY ZONE OF THE IAL (PLANE STRAIN, SIMPLIFIED ELASTO-PLASTIC VS NON-LINEAR SOLUTIONS).

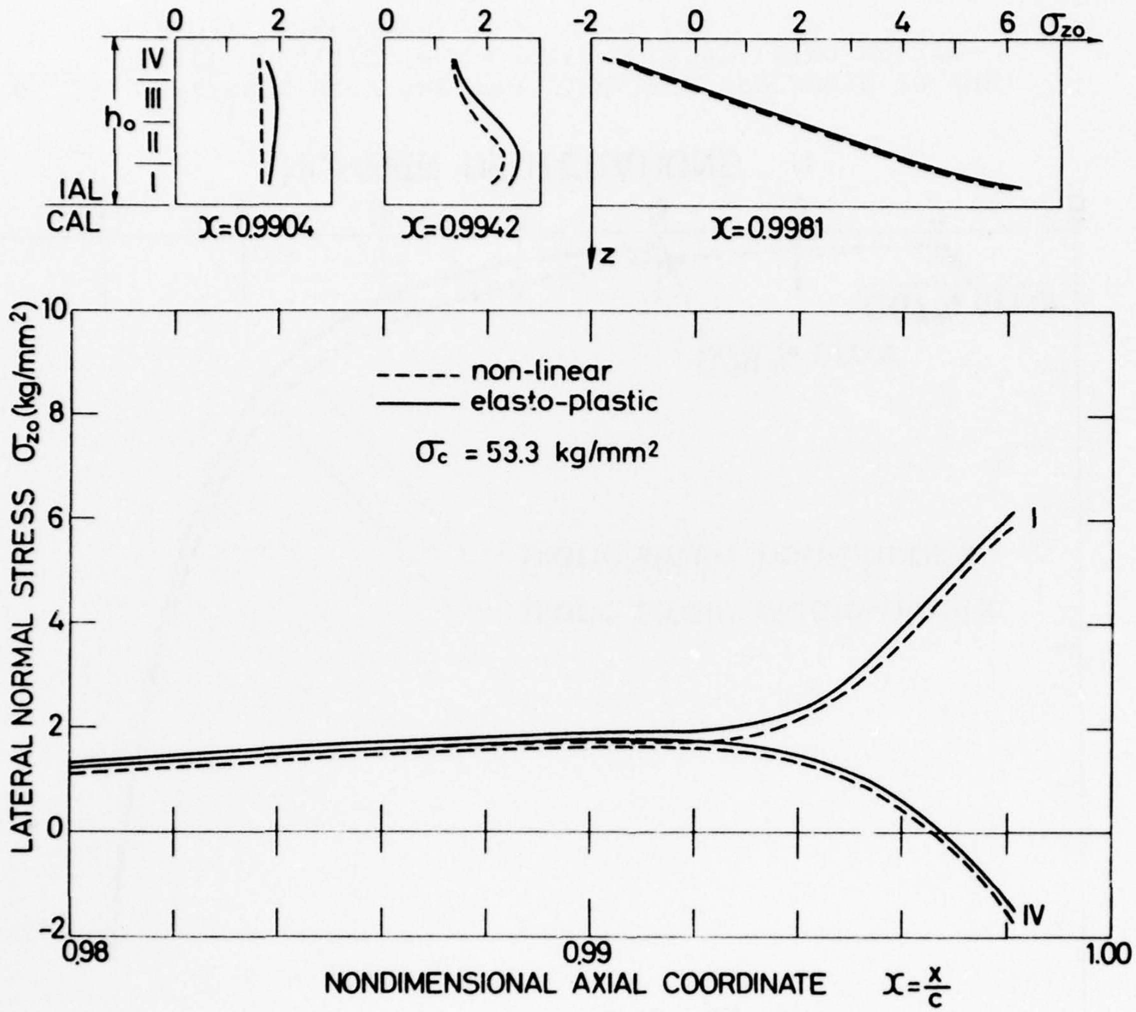

FIG. 34 LATERAL NORMAL STRESS DISTRIBUTION AT THE BOUNDARY ZONE OF THE IAL (PLANE STRAIN, SIMPLIFIED ELASTO-PLASTIC SOLUTION VS NON-LINEAR SOLUTIONS).

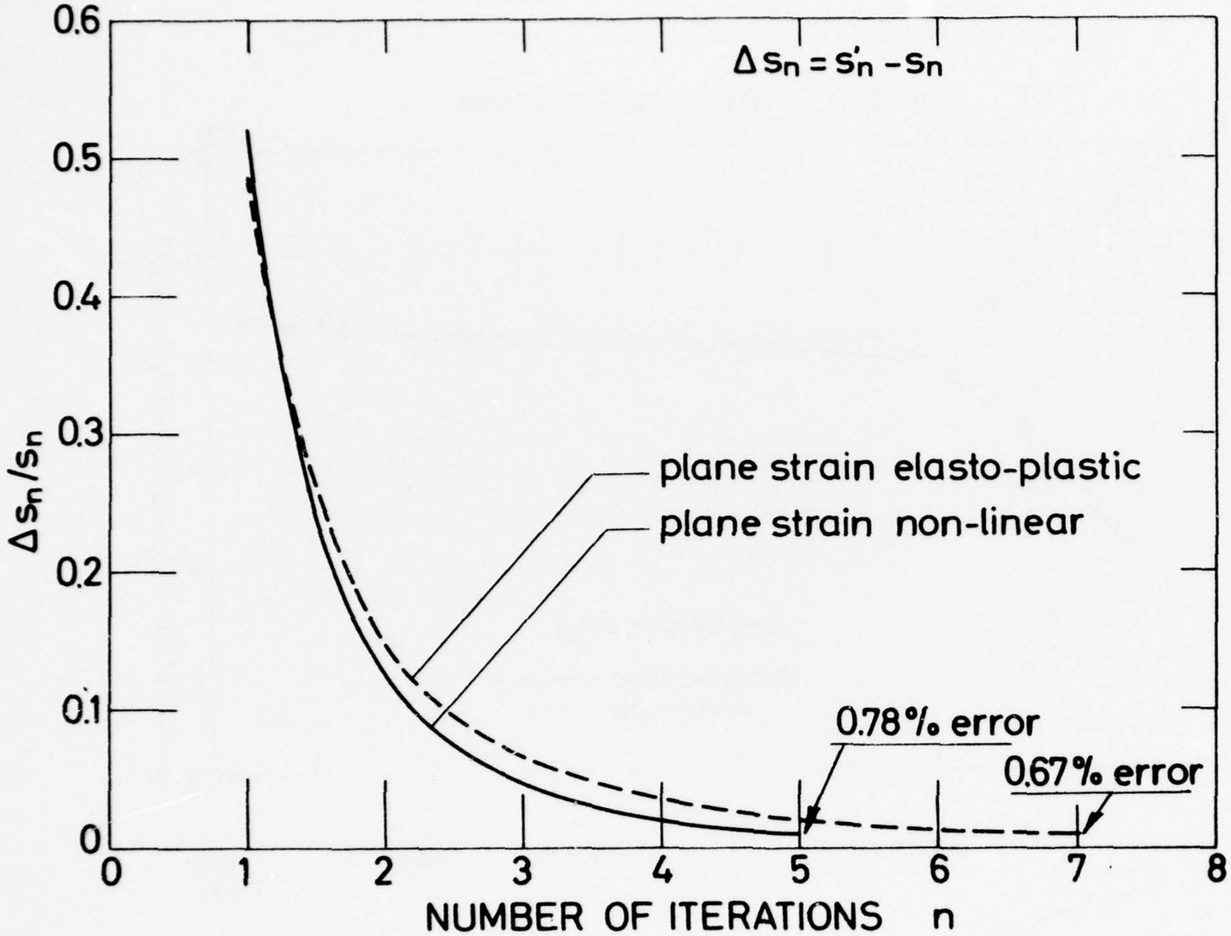

FIG. 35 CONVERGENCE OF THE FEM ITERATION PROCEDURE TO THE EXACT SOLUTION (NON-LINEAR VS SIMPLIFIED ELASTO-PLASTIC SOLUTIONS).

APPENDIX 1

PRINT-OUT OF TYPICAL FINITE ELEMENT PROGRAM FOR STRESS DISTRIBUTION IN AN INTERLAMINAR ADHESIVE LAYER WITHIN A DOUBLER MODEL.

JAN 73)   OS/360 FORTRAN H

```
FILER OPTIONS - NAME=  MAIN,OPT=02,LINECNT=60,SIZE=0000K,
                SOURCE,EBCDIC,NOLIST,NODECK,LOAD,NOMAP,NOEDIT,ID,NOXREF
C
C TWO DIMENSION PLAN STRAIN/STRESS FINITE ELEMENT PROGRAM
C FOR GENERAL MATERIAL
C
      REAL*8 TITLE(9)
      COMMON NNP,NEL,NMAT,NSLC,NCET,NBODY,MTYP,IE(200,5),RO(10),TH(10),
     1ET(10),UT(10),GGT(10),E1T(10),E2T(10),U12T(10),U21T(10),G12T(10),
     2GO(3,3),OM(3,3,10),E,U,GG,E1,E2,U12,U21,G12,GOT(3,3,10),
     3X(200),Y(200),ULX(200),VLY(200),KODE(200),ISC(20),JSC(20),
     4SURTRX(20,2),SURTRY(20,2),EE(10)
      COMMON/ONE/OK(10,10),Q(10),B(3,10),C(3,3),PT(3,6),XQ(5),YQ(5)
      COMMON /TWO/ IBAND,NEQ, R(400), AK(400,50)
      DATA MAXEL, MAXNP, MAXMAT, MAXBW, MAXSLC
     1     /  200,    200,     10,    50,     20/
 9999 READ 100,NPROB, (TITLE(I),I=1,9)
         IF(NPROB.LE.0) GO TO 999
 1020 PRINT 200,NPROB,(TITLE(I),I=1,9)
         CALL DATAIN (MAXEL,MAXNP,MAXMAT,MAXSLC,ISTOP)
              MAXDOF = 2*MAXNP
              MAXDIF = 0
         DO 1 I=1,NEL
         DO 1 J=1,4
         DO 1 K=1,4
              LL= IABS(IE(I,J)- IE(I,K))
         IF(LL.GT.MAXDIF) MAXDIF = LL
    1    CONTINUE
              IBAND = 2*(MAXDIF + 1)
              NEQ = 2*NNP
         IF(IBAND.GT.MAXBW) GO TO 900
         IF(ISTOP.GT.0) GO TO 999
         CALL ASEMBL(ISTOP)
         IF(ISTOP.GT.0) GO TO 999
         CALL BANSOL(1,AK,R,NEQ,IBAND,MAXDOF,MAXBW)
         CALL BANSOL(2,AK,R,NEQ,IBAND,MAXDOF,MAXBW)
      PRINT 300, (I,R(2*I-1),R(2*I),I=1,NNP)
         CALL STRESS
         GO TO 9999
  900 PRINT 901, IBAND, MAXBW
      GO TO 9999
  100 FORMAT( I5,3X,9A8 )
  200 FORMAT( /8H1PROBLEM,I5,3H.. ,9A8 )
  300 FORMAT(37H1OUTPUT TABLE 1.. NODAL DISPLACEMENTS //
     1        13X,4HNODE, 9X, 11HU = X-DISP.,9X,11HV = Y-DISP./
     2       (5X,I12,2E20.8))
  901 FORMAT(///12H BANDWIDTH =,I4,25H EXCEEDS MAX, ALLOWABLE =,I4//
     1 30H GO ON TO NEXT PROBLEM          )
  999 STOP
      END
```

```
.AN 73 )                                   OS/360  FORTRAN H

ILER OPTIONS - NAME=  MAIN,OPT=02,LINECNT=60,SIZE=0000K,
                SOURCE,EBCDIC,NOLIST,NODECK,LOAD,NOMAP,NOEDIT,ID,NOXREF
      SUBROUTINE  MATERP
      COMMON NNP,NEL,NMAT,NSLC,NOPT,NBODY,MTYP,IE(200,5),RO(10),TH(10),
     1ET(10),UT(10),GGT(10),E1T(10),E2T(10),U12T(10),U21T(10),G12T(10),
     2GG(3,3),QM(3,3,10),E,U,GG,E1,E2,U12,U21,G12,QQT(3,3,10),
     3X(200),Y(200),ULX(200),VLY(200),KODE(200),ISC(20),JSC(20),
     4SURTRX(20,2),SURTRY(20,2),EF(10)
      DO 250 IMAT=1,NMAT
      E=ET(IMAT)
      U=UT(IMAT)
      GG=GGT(IMAT)
      E1=E1T(IMAT)
      E2=E2T(IMAT)
      U12=U12T(IMAT)
      U21=U21T(IMAT)
      G12=G12T(IMAT)
      DO 350 I=1,3
      DO 350 J=1,3
  350 GG(I,J)=QQT(I,J,IMAT)
      IF ( E .EQ. 0. .AND.GG .EQ. 0. ) GO TO 500
      IF ( E .EQ. 0. ) GO TO 300
      IF ( U .EQ. 0. ) GO TO 200
      IF (GG .EQ. 0. )GG = E*0.5/(1.+U)
      GO TO  400
  200 IF (GG .NE. 0. ) U = 1. - E*0.5/GG
      GO TO  400
  300 IF ( U .EQ. 0. ) GO TO 400
      E = 2.*(1.+U)*GG
  400 IF(NOPT.EQ.1)GO TO 450
      GQ(1,1) = E/(1.-U*U)
      GQ(2,1) = U*QG(1,1)
      GG(3,3) = GG
      GG(2,2) = QQ(1,1)
      GO  TO 1000
  450 GQ(1,1)=E*(1-U)/((1+U)*(1-2*U))
      GQ(2,1)=E*U/((1+U)*(1-2*U))
      GQ(2,2)=QQ(1,1)
      GG(3,3)=GG
      GO TO 1000
  500 IF ( E1 .EQ. 0. .AND.  E2 .EQ. 0. ) GO TO 1000
      IF ( U12 .EQ. 0. ) GO TO 700
      IF ( U21 .EQ. 0. ) U21 = U12*E2/E1
      GO TO 800
  700 U12 = U21*E1/E2
  800 GQ(1,1) = E1/(1.-U12*U21)
      GG(2,1) = U21*QQ(1,1)
      GG(2,2) = E2/(1.-U12*U21)
      GQ(3,3) = G12
 1000 DO   1200 I=1,3
      DO   1200 J=1,I
      QM(I,J,IMAT)=GQ(I,J)
      QM(J,I,IMAT)=GQ(I,J)
 1200 CONTINUE
  250 CONTINUE
      RETURN
      END
```

BEST AVAILABLE COPY

JAN 73)   OS/360 FORTRAN H

```
FILER OPTIONS - NAME=  MAIN,OPT=02,LINECNT=60,SIZE=0000K,
                SOURCE,EBCDIC,NOLIST,NODECK,LOAD,NOMAP,NOEDIT,ID,NOXREF
      SUBROUTINE DATAIN(       MAXEL,MAXNP,MAXMAT,MAXSLC,ISTOP)
      COMMON NNP,NEL,NMAT,NSLC,NCPT,NBODY,NTYP,IE(200,5),RO(10),TH(10),
     1ET(10),UT(10),GGT(10),E1T(10),E2T(10),U12T(10),U21T(10),G12T(10),
     2GG(3,3),QM(3,3,10),E,U,GG,E1,E2,U12,U21,G12,QQT(3,3,10),
     3X(200),Y(200),ULX(200),VLY(200),KODE(200),ISC(20),JSC(20),
     4SURTRX(20,2),SURTRY(20,2),EF(10)
C
      ISTOP = 0
      READ 1,NNP,NEL,NMAT,NSLC,NCPT,NBODY
C
      PRINT 100,NNP,NEL,NMAT,NSLC,NCPT,NBODY
         IF(NNP.LE.MAXNP) GO TO 201
               ISTOP = ISTOP + 1
      PRINT 251, MAXNP
  201    IF(NEL.LE.MAXEL) GO TO 202
               ISTOP = ISTOP + 1
      PRINT 252, MAXEL
  202    IF(NMAT.LE.MAXMAT) GO TO 203
               ISTOP = ISTOP + 1
      PRINT 253, MAXMAT
  203    IF(NSLC.LE.MAXSLC) GO TO 204
               ISTOP = ISTOP + 1
      PRINT 254, MAXSLC
  204    IF(ISTOP.EQ.0) GO TO 205
      PRINT 255, ISTOP
      STOP
C
  205 READ 2, (RO(I),TH(I),I=1,NMAT)
      PRINT 101
      PRINT 51, (I,RO(I),TH(I),I=1,NMAT)
      READ 10,(ET(I),UT(I),GGT(I),E1T(I),E2T(I),U12T(I),U21T(I),
     1G12T(I),I=1,NMAT)
      PRINT 80, (I,ET(I),UT(I),GGT(I),E1T(I),E2T(I),U12T(I),U21T(I),
     1G12T(I),I=1,NMAT)
      DO 150 IMAT=1,NMAT
      DO 150 I=1,3
      READ 11, (QQT(I,J,IMAT),J=1,3)
      PRINT 81, (QQT(I,J,IMAT),J=1,3)
  150 CONTINUE
      CALL MATERP
       DO 550 IMAT=1,NMAT
      DO 550 I=1,3
      PRINT 82, (QM(I,J,IMAT),J=1,3)
  550 CONTINUE
      PRINT 103
               N=1
    5 READ 3, M,KODE(M),X(M),Y(M),ULX(M),VLY(M)
         IF(M-N)4,6,7
    4 PRINT 105, M
      PRINT 52,M,KODE(M), X(M),Y(M),ULX(M),VLY(M)
               ISTOP= ISTOP +1
         GO TO 5
    7          DF = M + 1 - N
               RX=(X(M)-X(N-1))/DF
               RY=(Y(M)-Y(N-1))/DF
    8          KODE(N)=0
```

```
                X(N)=X(N-1)+RX
                Y(N)=Y(N-1)+RY
                ULX(N)=0.0
                VLY(N)=0.0
    6 PRINT 52,N,KODE(N),X(N),Y(N),ULX(N),VLY(N)
                N=N+1
          IF(M-N)9,6,8
    9     IF(N.LE.NNP) GO TO 5
      PRINT 106
   13           L=0
   14 READ 15, M,(IE(M,I),I=1,5)
   16           L=L+1
          IF(M-L)117,17,18
  117 PRINT 118,M
      PRINT 53,M, (IE(M,I), I=1,5)
                ISTOP=ISTOP+1
          GO TO 14
   18           IE(L,1)= IE(L-1,1)+1
                IE(L,2)= IE(L-1,2)+1
                IE(L,3)=IE(L-1,3)+1
                IE(L,4)=IE(L-1,4)+1
                IE(L,5)=IE(L-1,5)
   17 PRINT 53, L,(IE(L,I),I=1,5)
          IF(M-L)20,20,16
   20     IF(NEL-L)21,21,14
   21     CONTINUE
          IF(NSLC.EQ.0) GO TO 31
   30 PRINT 108
          DO  40 L=1,NSLC
      READ 41,ISC(L),JSC(L),SURTRX(L,1),SURTRX(L,2),SURTRY(L,1),
     1 SURTRY(L,2)
   40 PRINT 42,ISC(L),JSC(L),SURTRX(L,1),SURTRX(L,2),SURTRY(L,1),
     1 SURTRY(L,2)
   31     IF(ISTOP.EQ.0) GO TO 999
      PRINT 900, ISTOP
C
    1 FORMAT(6I5)
  100 FORMAT(35H0INPUT TABLE 1.. BASIC PARAMETERS    //
     1          5X, 40H NUMBER OF NODAL POINTS. . . . . . . . . ..,I5/
     2          5X, 40H NUMBER OF ELEMENTS. . . . . . . . . . . ..,I5/
     3          5X, 40H NUMBER OF DIFFERENT MATERIALS . . . . . ..,I5/
     4          5X, 40H NUMBER OF SURFACE LOAD CARDS. . . . . . ..,I5/
     5          5X, 40H 1 = PLANE STRAIN, 2 = PLANE STRESS. . ..,I5/
     6          5X, 40H BODY FORCES(1 = IN -Y DIREC., 0 = NONE),I5)
  251 FORMAT(////33H TOO MANY NODAL POINTS, MAXIMUM =, I5)
  252 FORMAT(////30H TOO MANY ELEMENTS, MAXIMUM = ,I5)
  253 FORMAT(////30H TOO MANY MATERIALS, MAXIMUM =,I5)
  254 FORMAT(////40H TOO MANY SURFACE LOAD CARDS, MAXIMUM = ,I5)
  255 FORMAT(////28H EXECUTION HALTED BECAUSE OF,I5,13H FATAL ERRORS/)
    2 FORMAT(2E10.3)
  101 FORMAT(36H0INPUT TABLE 2.. MATERIAL PROPERTIES //
     1          10H   MATERIAL,5X,10HMODULUS OF,6X,9HPOISSON'S,7X,
     28HMATERIAL,7X,  8HMATERIAL /
     34X,6HNUMBER,5X,10HELASTICITY,8X,7H  RATIO,8X,7HDENSITY,6X,
     49HTHICKNESS )
   51 FORMAT(I10,2F15.4)
   10 FORMAT(8E10.3)
   80 FORMAT(I10,8F15.4)
```



```
   11 FORMAT(3E10.3)
   81 FORMAT(3E10.3)
   82 FORMAT(3E10.3)
  103 FORMAT(34H1INPUT TABLE 3.. NODAL POINT DATA //
    1          5X,5HNODAL,48X,7HX-DISP.,8X,7HY-DISP./
    25X,5HPOINT,6X,4HTYPE,14X,1HX,14X,1HY,8X,7HOR LOAD,8X,7HOR LOAD)
    3 FORMAT(2I5,4F10.3)
  105 FORMAT(5X,17HERROR IN CARD NO.,I5/)
   52 FORMAT(2I10,4E15.4)
  106 FORMAT(34H1INPUT TABLE 4.. ELEMENT DATA       //
    1          11X,31HGLOBAL INDICES OF ELEMENT NODES/3X,7HELEMENT,
    27X,1H1,7X,1H2,7X,1H3,7X,1H4,2X,8HMATERIAL)
  118 FORMAT( 5X, 25HERROR IN ELEMENT CARD NO.,I5 )
   15 FORMAT(6I5)
   53 FORMAT(I10,4I8,I10)
  108 FORMAT(37H1INPUT TABLE 5.. SURFACE LOADING DATA  //
    117X, 33HSURFACE LOAD INTENSITIES AT NODES/
    24X,6HNODE I,4X,6HNODE J,10X,2HXI,10X,2HXJ,10X,2HYI,10X,2HYJ)
   41 FORMAT(2I5,4F10.3)
   42 FORMAT(2I10,4E12.4)
  900 FORMAT(///45H ASSEMBLY AND SOLUTION WILL NOT BE PERFORMED.,I5,
    121H  FATAL CARD ERRORS      )
  999 RETURN
      END
```

```
JAN 73 )                              OS/360  FORTRAN H

PILER OPTIONS - NAME=  MAIN,OPT=02,LINECNT=60,SIZE=0000K,
                SOURCE,EBCDIC,NOLIST,NODECK,LOAD,NOMAP,NOEDIT,ID,NOXREF
      SUBROUTINE GEOMBC(U,N)
      COMMON/TWO/ IBAND,NEQ,R(400), AK(400,50)
C  THIS SUBROUTINE MODIFIES THE ASSEMBLAGE STIFFNESS AND LOADS FOR THE
C  PRESCRIBED DISPLACEMENT U AT DEGREE OF FREEDOM N, EQ.(6-18B). (REF.1)
         DO 100 M=2,IBAND
              K = N - M + 1
              IF(K.LE.0) GO TO 50
              R(K) = R(K) - AK(K,M)*U
              AK(K,M) = 0.0
   50         K = N + M - 1
              IF(K.GT.NEQ) GO TO 100
              R(K) = R(K) - AK(N,M)*U
              AK(N,M) = 0.0
  100    CONTINUE
              AK(N,1) = 1.0
              R(N) = U
      RETURN
      END
```

AN 73)   OS/360 FORTRAN H

```
ILER OPTIONS - NAME=  MAIN,OPT=02,LINECNT=60,SIZE=0000K,
               SOURCE,EBCDIC,NOLIST,NODECK,LOAD,NOMAP,NOEDIT,ID,NOXREF
      SUBROUTINE  ASEMBL(ISTOP)
      COMMON NNP,NEL,NMAT,NSLC,NCPT,NBODY,MTYP,IE(200,5),RO(10),TH(10),
     1ET(10),UT(10),GGT(10),E1T(10),E2T(10),U12T(10),U21T(10),G12T(10),
     2QQ(3,3),QM(3,3,10),E,U,GG,E1,E2,U12,U21,G12,QQT(3,3,10),
     3X(200),Y(200),ULX(200),VLY(200),KODE(200),ISC(20),JSC(20),
     4SURTRX(20,2),SURTRY(20,2),EF(10)
      COMMON/ONE/ QK(10,10),Q(10),B(3,10),C(3,3),BT(3,6),XQ(5),YQ(5)
      COMMON/TWO/ IBAND,NEQ,R(400), AK(400,50)
      DIMENSION LP(8)
C
      REWIND 1
            ISTOP = 0
            BT(1,4) = 0.0
            BT(1,5) = 0.0
            BT(1,6) = 0.0
            BT(2,1) = 0.0
            BT(2,2) = 0.0
            BT(2,3) = 0.0
         DO  2 I=1,NEQ
            R(I)=0.0
         DO  2 J =1,IBAND
    2       AK(I,J) = 0.0
         DO 10 M=1,NEL
         IF(IE(M,5).GT.0) GO TO 11
            ISTOP = ISTOP + 1
         GO TO 10
   11    CALL QUAD(M,AREA)
         IF(AREA.GT.0.0) GO TO 16
            ISTOP = ISTOP + 1
      PRINT 20,M
   16    IF(IE(M,3).EQ.IE(M,4)) GO TO 26
         DO 31 J = 1,2
            IJ= 10-J
            IK= IJ+1
            PIVOT = QK(IK,IK)
         DO 32 K= 1,IJ
            F = QK(IK,K)/PIVOT
            QK(IK,K)=F
         DO 33 I=K,IJ
            QK(I,K)=QK(I,K)- F*QK(I,IK)
   33       QK(K,I) = QK(I,K)
   32       Q(K) =Q(K)-QK(IK,K)*Q(IK)
   31       Q(IK) =Q(IK)/PIVOT
   26 WRITE (1) ((QK(I,J),J=1,10),I=9,10), Q(9), Q(10),
     1((B(I,J),J=1,10),I=1,3),((C(I,J),J=1,3),I=1,3),XQ(5),YQ(5)
            LIM=8
         IF(IE(M,3).EQ.IE(M,4)) LIM = 6
         DO 40 I=2,LIM,2
            IJ = I/2
            LP(I-1) = 2*IE(M,IJ) - 1
   40       LP(I) = 2*IE(M,IJ)
         DO 50 LL=1,LIM
            I = LP(LL)
            R(I) = R(I) + Q(LL)
         DO 50 MM=1,LIM
            J = LP(MM) - I + 1
```



```
          IF (J.LE. 0 ) GO TO 50
               AK(I,J)= AK(I,J)+ GK(LL,MM)
   50     CONTINUE
   10     CONTINUE
          DO 55 N=1,NNP
          IF(KODE(N).EQ.3) GO TO 55
               K=2*N
          IF( KODE(N).EQ.1) GO TO 57
               R(K-1) = R(K-1) + ULX(N)
          IF(KODE(N).NE.0) GO TO 55
   57          R(K) = R(K) + VLY(N)
   55     CONTINUE
          IF(NSLC.EQ.0) GO TO 60
          DO 61 L = 1,NSLC
               I = ISC(L)
               J = JSC(L)
               II=2*I
               JJ=2*J
               DX = X(J) - X(I)
               DY = Y(J) - Y(I)
               EL = SQRT(DX*DX + DY*DY)
               PXI=SURTRX(L,1)*EL
               PXJ=SURTRX(L,2)*EL
               PYI=SURTRY(L,1)*EL
               PYJ=SURTRY(L,2)*EL
               R(II-1) = R(II-1) + PXI/3.0 + PXJ/6.0
               R(JJ-1) = R(JJ-1) + PXI/6.0 + PXJ/6.0
               R(II)=R(II)+ PYI/3.0 + PYJ/6.0
               R(JJ)= R(JJ) + PYI/6.0 + PYJ/3.0
   61     CONTINUE
   60     DO 70 M=1,NNP
          IF(KODE(M).GE.0.AND.KODE(M).LE.3) GO TO 72
               ISTOP = ISTOP + 1
          GO TO 70
   72     IF(KODE(M).EQ.0) GO TO 70
          IF(KODE(M).EQ.2) GO TO 71
          CALL GEOMBC(ULX(M),2*M-1)
          IF(KODE(M).EQ.1) GO TO 70
   71     CALL GEOMBC(VLY(M),2*M)
   70     CONTINUE
      ENDFILE 1
          IF(ISTOP.EQ.0) GO TO 81
      PRINT 100, ISTOP
   20 FORMAT(/5X,17H AREA OF ELEMENT ,I5,14H  IS NEGATIVE  /)
  100 FORMAT(////42H SOLUTION WILL NOT BE PERFORMED BECAUSE OF  ,I5,
     1 15H   DATA ERRORS       /)
   81 RETURN
      END
```

```
IN 73 )                                  OS/360  FORTRAN H

LER OPTIONS - NAME=  MAIN,OPT=02,LINECNT=60,SIZE=0000K,
              SOURCE,EBCDIC,NOLIST,NODECK,LOAD,NOMAP,NOEDIT,ID,NOXREF
      SUBROUTINE QUAD(M,TOTALA)
      COMMON NNP,NEL,NMAT,NSLC,NCFT,NBODY,MTYP,IE(200,5),RO(10),TH(10),
     1ET(10),UT(10),GGT(10),E1T(10),E2T(10),U12T(10),U21T(10),G12T(10),
     2GG(3,3),QM(3,3,10),E,U,GG,E1,E2,U12,U21,G12,QQT(3,3,10),
     3X(200),Y(200),ULX(200),VLY(200),KODE(200),ISC(20),JSC(20),
     4SURTRX(20,2),SURTRY(20,2),EF(10)
      COMMON/ONE/ QK(10,10),Q(10),B(3,10),C(3,3),BT(3,6),XQ(5),YQ(5)
      COMMON/TWO/ IBAND,NEG,R(400), AK(400,50)
C
               I= IE(M,1)
               J= IE(M,2)
               K= IE(M,3)
               L= IE(M,4)
               MTYP = IE(M,5)
               TOTALA = 0.0
      IF(NMAT.EQ.1.AND.M.GT.1) GO TO 5
      C(1,1)=QM(1,1,MTYP)
      C(1,2)=QM(1,2,MTYP)
      C(1,3)=QM(1,3,MTYP)
      C(2,1)=QM(2,1,MTYP)
      C(2,2)=QM(2,2,MTYP)
      C(2,3)=QM(2,3,MTYP)
      C(3,1)=QM(3,1,MTYP)
      C(3,2)=QM(3,2,MTYP)
      C(3,3)=QM(3,3,MTYP)
    5          LIM = 4
           IF(K.EQ.L) LIM = 3
               XQ(5) = 0.0
               YQ(5) = 0.0
           DO 10 N=1,LIM
               NN = IE(M,N)
               XQ(N) = X(NN)
               YQ(N) = Y(NN)
               XQ(5) = XQ(5) + X(NN)/FLOAT(LIM)
   10          YQ(5) = YQ(5) + Y(NN)/FLOAT(LIM)
           DO 13 II =1,10
               Q(II)=0.0
           DO 12 JJ = 1,10
   12          QK(II,JJ)=0.0
           DO 13 JJ=1,3
   13          B(JJ,II) = 0.0
           IF(K.NE.L) GO TO 15
      CALL CST(1,2,3,TOTALA)
           GO TO 999
   15 CALL CST(1,2,5,AREA)
               TOTALA = TOTALA + AREA
      CALL CST(2,3,5,AREA)
               TOTALA = TOTALA + AREA
      CALL CST(3,4,5,AREA)
               TOTALA = TOTALA + AREA
      CALL CST(4,1,5,AREA)
               TOTALA = TOTALA + AREA
  999 RETURN
      END
```



```
 N 73 )                               OS/360  FORTRAN H

ILER OPTIONS - NAME=  MAIN,OPT=02,LINECNT=60,SIZE=0000K,
               SOURCE,EBCDIC,NOLIST,NODECK,LOAD,NOMAP,NOEDIT,ID,NOXREF
      SUBROUTINE  CST(I,J,K,AREA)
      COMMON NNP,NEL,NMAT,NSLC,NCPT,NBODY,MTYP,IE(200,5),RO(10),TH(10),
     1ET(10),UT(10),GGT(10),E1T(10),E2T(10),U12T(10),U21T(10),G12T(10),
     2GG(3,3),QM(3,3,10),E,U,GG,E1,E2,U12,U21,G12,QQT(3,3,10),
     3X(200),Y(200),ULX(200),VLY(200),KODE(200),ISC(20),JSC(20),
     4SURTRX(20,2),SURTRY(20,2),EE(10)
      COMMON/ONE/ GK(10,10),Q(10),B(3,10),C(3,3),BT(3,6),XQ(5),YQ(5)
      COMMON/TWO/ IBAND,NEQ,R(400), AK(400,50)
      DIMENSION CB(3,6),LC(6),LT(3),TK(6,6)
C
                LT(1)= I
                LT(2)= J
                LT(3)= K
                BT(1,1)= YQ(J)-YQ(K)
                BT(1,2)= YQ(K)-YQ(I)
                BT(1,3) = YQ(I)-YQ(J)
                BT(2,4)=XQ(K)-XQ(J)
                BT(2,5) = XQ (I)-XQ(K)
                BT(2,6) = XQ(J) -XQ(I)
                BT(3,1)=BT(2,4)
                BT(3,2) = BT(2,5)
                BT(3,3) = BT(2,6)
                BT(3,4) = BT(1,1)
                BT(3,5)= BT(1,2)
                BT(3,6)= BT(1,3)
                AREA =(BT(2,4)*BT(1,3) - BT(2,6)*BT(1,1))/2.0
           DO 10 II=1,3
           DO 10JJ = 1,6
                CB(II,JJ) = 0.0
      DO 10 KK = 1,3
   10           CB(II,JJ) = CB(II,JJ) + C (II,KK)*BT(KK,JJ)
           DO 12 II = 1,6
           DO 12 JJ = 1,6
                TK(II,JJ)=0.0
           DO 12 KK=1,3
   12           TK(II,JJ)=    TK(II,JJ)+BT(KK,II)*CB(KK,JJ)
           DO 15 II=1,3
                LC(II) = 2*LT(II) - 1
   15           LC(II+3) = 2*LT(II)
           DO 30 II=1,6
                LL = LC(II)
                FK = 1.0/(4.0*AREA)
                FB = 2.0*FK
           DO 20 JJ=1,6
                MM = LC(JJ)
   20           GK(LL,MM) = GK(LL,MM) + TK(II,JJ)*TH(MTYP)*FK
           DO 30 JJ = 1,3
   30           B(JJ,LL) = B(JJ,LL) + BT(JJ,II)*FB
           IF(NBODY.EQ.0) GO TO 999
                TBODYF =  AREA* RO(MTYP)*  TH(MTYP)
                BODYF  = -TBODYF/3.0
           DO 35 II=1,3
                JJ= 2* LT(II)
   35           Q(JJ)= Q(JJ)+ BODYF
  999 RETURN
      END
```

```
AN 73 )                              OS/360  FORTRAN H

ILER OPTIONS - NAME=  MAIN,OPT=02,LINECNT=60,SIZE=0000K,
               SOURCE,EBCDIC,NOLIST,NODECK,LOAD,NOMAP,NOEDIT,ID,NOXREF
      SUBROUTINE STRESS
      COMMON NNP,NEL,NMAT,NSLC,NOPT,NBODY,MTYP,IE(200,5),RO(10),TH(10),
     1ET(10),UT(10),GGT(10),E1T(10),E2T(10),U12T(10),U21T(10),G12T(10),
     2QQ(3,3),QM(3,3,10),E,U,GG,E1,E2,U12,U21,G12,QQT(3,3,10),
     3X(200),Y(200),ULX(200),VLY(200),KODE(200),ISC(20),JSC(20),
     4SURTRX(20,2),SURTRY(20,2),EP(10)
      COMMON/ONE/ QK(10,10),Q(10),B(3,10),C(3,3),BT(3,6),XQ(5),YQ(5)
      COMMON/TWO/ IBAND,NEG,R(400), AK(400,50)
      DIMENSION SIG(6)
C
      REWIND 1
      PRINT 300
           NOLINE = 47
         DO 5 M=1,NEL
      READ(1) ((QK(I,J),J=1,10),I=1,2),  Q(9), Q(10),
     1    ((B(I,J),J=1,10),I=1,3), ((C(I,J),J=1,3),I=1,3), XC,YC
           LIM = 4
         IF(IE(M,3).EQ.IE(M,4)) LIM = 3
         DO 10 I=1,LIM
           II = 2*I
           JJ = 2*IE(M,I)
           Q(II-1) = R(JJ-1)
   10      Q(II) = R(JJ)
         IF(LIM.EQ.3) GO TO 16
         DO 15 K=1,2
           JK = K + 8
           IK = JK - 1
         DO 15 L=1,IK
   15      Q(JK) = Q(JK) - QK(K,L)*Q(L)
           LIM = 10
           FAC = 0.25
         GO TO 17
   16      LIM = 6
           FAC = 1.0
   17    DO 20 I=1,3
         EP(I)=0.0
         DO 20 J=1, LIM
   20     EP(I)=EP(I)+B(I,J)*Q(J)*FAC
         DO 30 I=1,3
           SIG(I) = 0.0
         DO 30 J=1,3
   30     SIG(I)=SIG(I)+C(I,J)*EP(J)
           SP = (SIG(1)+SIG(2))/2.0
           SM = (SIG(1)-SIG(2))/2.0
           DS = SQRT(SM*SM+SIG(3)*SIG(3))
           SIG(4) = SP + DS
           SIG(5) = SP - DS
           SIG(6) = 0.0
         IF(SIG(3).NE.0.0.AND.SM.NE.0.0) SIG(6) = 28.648*ATAN2(SIG(3),
     1                                                              SM)
         IF(NOLINE.GT.0) GO TO 54
      PRINT 1000
           NOLINE = 49
   54      NOLINE = NOLINE - 1
    5 PRINT 1010, M,XC,YC,(SIG(I),I=1,6)
      ENDFILE 1
```



```
  300 FORMAT(47H1OUTPUT TABLE 2.. STRESSES AT ELEMENT CENTROIDS //
     11X,7HELEMENT,9X,1HX,9X,1HY,4X,8HSIGMA(X),4X,8HSIGMA(Y),4X,
     28HTAU(X,Y),4X,8HSIGMA(1),4X,8HSIGMA(2), 7X,5HANGLE )
 1000 FORMAT(1H1,    7HELEMENT,9X,1HX,9X,1HY,4X8HSIGMA(X),4X,8HSIGMA(Y),
     14X,8HTAU(X,Y),4X,8HSIGMA(1),4X,8HSIGMA(2), 7X,5HANGLE )
 1010 FORMAT(I8, 2F10.2,1P6E12.4)
      RETURN
      END
```

```
JAN 73 )                              OS/360  FORTRAN H

PILER OPTIONS - NAME=  MAIN,OPT=02,LINECNT=60,SIZE=0000K,
                SOURCE,EBCDIC,NOLIST,NODECK,LOAD,NOMAP,NOEDIT,ID,NOXREF
      SUBROUTINE BANSOL(KKK,AK,R,NEQ,IBAND,NDIM,MDIM)
C SYMMETRIC BAND MATRIX EQUATION SOLVER.  (REF. 2)
C
C KKK = 1 TRIANGULARIZES THE BAND MATRIX AK, EQ. (2-2)
C KKK = 2 SOLVES FOR RIGHT HAND SIDE R, SOLUTION RETURNS IN R, EQ.(2-3)
C
      DIMENSION AK(NDIM,MDIM), R(1)
                NRS = NEQ - 1
                NR = NEQ
           IF(KKK.EQ.2) GO TO 200
           DO 120 N= 1,NRS
                M= N-1
                MR = MIN0(IBAND,NR-M)
                PIVOT = AK(N,1)
           DO 120 L=2,MR
                CP= AK(N,L)/PIVOT
                I = M+L
                J = 0
           DO 110 K=L,MR
                J = J + 1
  110           AK(I,J)= AK(I,J) -CP*AK(N,K)
  120           AK(N,L) = CP
           GO TO 400
  200      DO 220 N=1,NRS
                M= N-1
                MR = MIN0(IBAND,NR-M)
                CP= R(N)
                R(N)=CP/AK(N,1)
           DO 220  L=2,MR
                I = M + L
  220           R(I)= R(I) - AK(N,L)*CP
                R(NR) = R(NR)/AK(NR,1)
           DO 320 I = 1,NRS
                N= NR- I
                M= N-1
                MR = MIN0(IBAND,NR-M)
           DO 320 K = 2,MR
                L = M+K
C   STORE COMPUTED DISPLACEMENTS IN LOAD VECTOR R
  320           R(N)= R(N)- AK(N,K)*R(L)
  400 RETURN
      END
```